

**EXPERIMENT ON WAVE OVERTOPPING AND  
OVERWASH OF BARE AND VEGETATED DUNES**

BY

CHRISTINE GRALHER, NOBUHISA KOBAYASHI

AND KIDEOK DO

RESEARCH REPORT NO. CACR-12-05

JUNE 2012



**CENTER FOR APPLIED COASTAL RESEARCH**

Ocean Engineering Laboratory  
University of Delaware  
Newark, Delaware 19716



## **ACKNOWLEDGMENTS**

This study was supported partly by the EU THESEUS Project and the U.S. Army Corps of Engineers Coastal and Hydraulics Laboratory under Contract No. W912HZ-11-P-0173.

The third writer was supported by the Basic Research Program (400-20100155) of the National Research Foundation, Ministry of Education, Science and Technology of Republic of Korea.



## TABLE OF CONTENTS

<b>LIST OF TABLES</b> . . . . .	<b>vi</b>
<b>LIST OF FIGURES</b> . . . . .	<b>xii</b>
<b>ABSTRACT</b> . . . . .	<b>xiv</b>
 <b>Chapter</b>	
<b>1 INTRODUCTION</b> . . . . .	<b>1</b>
<b>2 EXPERIMENT</b> . . . . .	<b>5</b>
2.1 Experimental Setup . . . . .	5
2.2 Test Overview . . . . .	9
2.2.1 Tested Nearshore Profiles . . . . .	9
2.2.2 Vegetation Modeling . . . . .	11
2.3 Test Procedure . . . . .	14
2.3.1 Wave Gauges . . . . .	17
2.3.2 Velocity Measurements . . . . .	18
<b>3 DATA ANALYSIS</b> . . . . .	<b>20</b>
3.1 Hydrodynamics . . . . .	20
3.1.1 Incident Wave Characteristics . . . . .	21
3.1.2 Free Surface Elevation and Wet Probability . . . . .	26
3.1.3 Velocity . . . . .	40
3.2 Morphology and Overwash . . . . .	47
3.2.1 Transport Rates . . . . .	47
3.2.2 Profile Evolution . . . . .	55
3.2.3 Erosion and Deposition . . . . .	59

<b>4 CONCLUSIONS . . . . .</b>	<b>70</b>
<b>REFERENCES . . . . .</b>	<b>72</b>
<b>Appendix</b>	
<b>TABULATED DATA . . . . .</b>	<b>75</b>

## LIST OF TABLES

2.1	Sediment characteristics. . . . .	7
2.2	Test overview and notations. . . . .	11
2.3	Location and classification of all wave gauges for all five tests. . . . .	18
2.4	Location of all three velocimeters for all five tests. . . . .	19
3.1	Incident wave characteristics at WG1 ( $x = 0\text{ m}$ ) for the 6 runs of the HB test. . . . .	22
3.2	Incident wave characteristics at WG1 ( $x = 0\text{ m}$ ) for the 6 runs of the HN test. . . . .	22
3.3	Incident wave characteristics at WG1 ( $x = 0\text{ m}$ ) for the 28 runs of the HW test. . . . .	23
3.4	Incident wave characteristics at WG1 ( $x = 0\text{ m}$ ) for the 3 runs of the LB test. . . . .	24
3.5	Incident wave characteristics at WG1 ( $x = 0\text{ m}$ ) for the 20 runs of the LW test. . . . .	25
3.6	Mean free-surface elevation $\bar{\eta}$ ( $cm$ ) at eight wave gauge locations for the 6 runs of the HB test. . . . .	29
3.7	Mean free-surface elevation $\bar{\eta}$ ( $cm$ ) at eight wave gauge locations for the 6 runs of the HN test. . . . .	30
3.8	Mean free-surface elevation $\bar{\eta}$ ( $cm$ ) at eight wave gauge locations for the 28 runs of the HW test. . . . .	31
3.9	Mean free-surface elevation $\bar{\eta}$ ( $cm$ ) at eight wave gauge locations for the 3 runs of the LB test. . . . .	32

3.10	Mean free-surface elevation $\bar{\eta}$ ( $cm$ ) at eight wave gauge locations for the 20 runs of the LW test. . . . .	33
3.11	Free-surface standard deviation $\sigma_{\eta}$ ( $cm$ ) at eight wave gauge locations for the 6 runs of the HB test. . . . .	34
3.12	Free-surface standard deviation $\sigma_{\eta}$ ( $cm$ ) at eight wave gauge locations for the 6 runs of the HN test. . . . .	35
3.13	Free-surface standard deviation $\sigma_{\eta}$ ( $cm$ ) at eight wave gauge locations for the 28 runs of the HW test. . . . .	36
3.14	Free-surface standard deviation $\sigma_{\eta}$ ( $cm$ ) at eight wave gauge locations for the 3 runs of the LB test. . . . .	37
3.15	Free-surface standard deviation $\sigma_{\eta}$ ( $cm$ ) at eight wave gauge locations for the 20 runs of the LW test. . . . .	38
3.16	Wet probability $P_w$ for WG8 for the high dune test series. . . . .	39
3.17	Mean cross-shore $\bar{u}$ and its standard deviation $\sigma_u$ of the 2D ADV co-located with WG5 at $x = 12.90 m$ , blue Vectrino co-located with WG6 at $x = 15.52 m$ and red Vectrino co-located with WG7 at $x = 17.07 m$ for the HB Test. . . . .	42
3.18	Mean cross-shore $\bar{u}$ and its standard deviation $\sigma_u$ of the 2D ADV co-located with WG5 at $x = 12.90 m$ , blue Vectrino co-located with WG6 at $x = 15.52 m$ and red Vectrino co-located with WG7 at $x = 17.07 m$ for the HN test. . . . .	43
3.19	Mean cross-shore $\bar{u}$ and its standard deviation $\sigma_u$ of the 2D ADV co-located with WG5 at $x = 12.90 m$ , blue Vectrino co-located with WG6 at $x = 15.52 m$ and red Vectrino co-located with WG7 at $x = 17.07 m$ for the HW test. . . . .	44
3.20	Mean cross-shore $\bar{u}$ and its standard deviation $\sigma_u$ of the 2D ADV co-located with WG5 at $x = 12.90 m$ , blue Vectrino co-located with WG6 at $x = 15.52 m$ and red Vectrino co-located with WG7 at $x = 17.07 m$ for the LB test. . . . .	45

3.21	Mean cross-shore $\bar{u}$ and its standard deviation $\sigma_u$ of the 2D ADV co-located with WG5 at $x = 12.90\text{ m}$ , blue Vectrino co-located with WG6 at $x = 15.52\text{ m}$ and red Vectrino co-located with WG7 at $x = 17.07\text{ m}$ for the LW test. . . . .	46
3.22	Measured sediment overwash rate ( $q_{bs}$ ), water overtopping rate ( $q_o$ ), and their ratio for the 6 runs of the HB test. . . . .	52
3.23	Measured sediment overwash rate ( $q_{bs}$ ), water overtopping rate ( $q_o$ ), and their ratio for the 6 runs of the HN test. . . . .	52
3.24	Measured sediment overwash rate ( $q_{bs}$ ), water overtopping rate ( $q_o$ ), and their ratio for the 28 runs of the HW test. . . . .	53
3.25	Measured sediment overwash rate ( $q_{bs}$ ), water overtopping rate ( $q_o$ ), and their ratio for the 3 runs of the LB test. . . . .	53
3.26	Measured sediment overwash rate ( $q_{bs}$ ), water overtopping rate ( $q_o$ ), and their ratio for the 20 runs of the LW test. . . . .	54
3.27	Cumulative values of the eroded ( $V_e$ ), deposited ( $V_d$ ) sand volume, and net erosion ( $V_c$ ) for the 6 runs of the HB test. Units are $cm^2$ because all values are given per unit width ( $cm^3/cm$ ). . . . .	60
3.28	Cumulative values of the eroded ( $V_e$ ), deposited ( $V_d$ ) sand volume, and net erosion ( $V_c$ ) for the 6 runs of the HN test. Units are $cm^2$ because all values are given per unit width ( $cm^3/cm$ ). . . . .	60
3.29	Cumulative values of the eroded ( $V_e$ ), deposited ( $V_d$ ) sand volume, and net erosion ( $V_c$ ) for the 28 runs of the HW test. Units are $cm^2$ because all values are given per unit width ( $cm^3/cm$ ). . . . .	61
3.30	Cumulative values of the eroded ( $V_e$ ), deposited ( $V_d$ ) sand volume, and net erosion ( $V_c$ ) for the 3 runs of the LB test. Units are $cm^2$ because all values are given per unit width ( $cm^3/cm$ ). . . . .	61
3.31	Cumulative values of the eroded ( $V_e$ ), deposited ( $V_d$ ) sand volume, and net erosion ( $V_c$ ) for the 20 runs of the LW test. Units are $cm^2$ because all values are given per unit width ( $cm^3/cm$ ). . . . .	62
3.32	Measured cumulative overwash ( $V_o$ ), offshore loss ( $V_L$ ) and net erosion ( $V_c$ ) and their ratios where volumes are given per unit width ( $cm^3/cm$ ) for the 6 runs of the HB test. . . . .	67

3.33	Measured cumulative overwash ( $V_o$ ), offshore loss ( $V_L$ ) and net erosion ( $V_c$ ) and their ratios where volumes are given per unit width ( $cm^3/cm$ ) for the 6 runs of the HN test. . . . .	67
3.34	Measured cumulative overwash ( $V_o$ ), offshore loss ( $V_L$ ) and net erosion ( $V_c$ ) and their ratios where volumes are given per unit width ( $cm^3/cm$ ) for the 28 runs of the HW test. . . . .	68
3.35	Measured cumulative overwash ( $V_o$ ), offshore loss ( $V_L$ ) and net erosion ( $V_c$ ) and their ratios where volumes are given per unit width ( $cm^3/cm$ ) for the 3 runs of the LB test. . . . .	69
3.36	Measured cumulative overwash ( $V_o$ ), offshore loss ( $V_L$ ) and net erosion ( $V_c$ ) and their ratios where volumes are given per unit width ( $cm^3/cm$ ) for the 20 runs of the LW test. . . . .	69
A.1	Spectrum and time series parameters for total waves at WG1 ( $x = 0 m$ ) for the 6 runs of the HB test. . . . .	75
A.2	Spectrum and time series parameters for total waves at WG1 ( $x = 0 m$ ) for the 6 runs of the HN test. . . . .	75
A.3	Spectrum and time series parameters for total waves at WG1 ( $x = 0 m$ ) for the 28 runs of the HW test. . . . .	76
A.4	Spectrum and time series parameters for total waves at WG1 ( $x = 0 m$ ) for the 3 runs of the LB test. . . . .	77
A.5	Spectrum and time series parameters for total waves at WG1 ( $x = 0 m$ ) for the 20 runs of the LW test. . . . .	77
A.6	Mean cross-shore $\bar{u}$ , and alongshore $\bar{v}$ velocity and their standard deviations of the 2D ADV co-located with WG5 at $x = 12.90 m$ for the HB test. . . . .	78
A.7	Mean cross-shore $\bar{u}$ , and alongshore $\bar{v}$ velocity and their standard deviations of the 2D ADV co-located with WG5 at $x = 12.90 m$ for the HN test. . . . .	78
A.8	Mean cross-shore $\bar{u}$ , and alongshore $\bar{v}$ velocity and their standard deviations of the 2D ADV co-located with WG5 at $x = 12.90 m$ for the HW test. . . . .	79

A.9	Mean cross-shore $\bar{u}$ , and alongshore $\bar{v}$ velocity and their standard deviations of the 2D ADV co-located with WG5 at $x = 12.90 m$ for the LB test. . . . .	80
A.10	Mean cross-shore $\bar{u}$ , and alongshore $\bar{v}$ velocity and their standard deviations of the 2D ADV co-located with WG5 at $x = 12.90 m$ for the LW test. . . . .	80
A.11	Mean cross-shore $\bar{u}$ , alongshore $\bar{v}$ , and vertical $\bar{w}$ velocity and their standard deviations of the blue Vectrino co-located with WG6 at $x = 15.52 m$ for the HB test. . . . .	81
A.12	Mean cross-shore $\bar{u}$ , alongshore $\bar{v}$ , and vertical $\bar{w}$ velocity and their standard deviations of the blue Vectrino co-located with WG6 at $x = 15.52 m$ for the HN test. . . . .	81
A.13	Mean cross-shore $\bar{u}$ , alongshore $\bar{v}$ , and vertical $\bar{w}$ velocity and their standard deviations of the blue Vectrino co-located with WG6 at $x = 15.52 m$ for the HW Test. . . . .	82
A.14	Mean cross-shore $\bar{u}$ , alongshore $\bar{v}$ , and vertical $\bar{w}$ velocity and their standard deviations of the blue Vectrino co-located with WG6 at $x = 15.52 m$ for the LB test. . . . .	83
A.15	Mean cross-shore $\bar{u}$ , alongshore $\bar{v}$ , and vertical $\bar{w}$ velocity and their standard deviations of the blue Vectrino at co-located with WG6 at $x = 15.52 m$ for the LW Test. . . . .	84
A.16	Mean cross-shore $\bar{u}$ , alongshore $\bar{v}$ , and vertical $\bar{w}$ velocity and their standard deviations of the red Vectrino co-located with WG7 at $x = 17.07 m$ for the HB test. . . . .	85
A.17	Mean cross-shore $\bar{u}$ , alongshore $\bar{v}$ , and vertical $\bar{w}$ velocity and their standard deviations of the red Vectrino co-located with WG7 at $x = 17.07 m$ for the HN test. . . . .	85
A.18	Mean cross-shore $\bar{u}$ , alongshore $\bar{v}$ , and vertical $\bar{w}$ velocity and their standard deviations of the red Vectrino co-located with WG7 at $x = 17.07 m$ for the HW test. . . . .	86
A.19	Mean cross-shore $\bar{u}$ , alongshore $\bar{v}$ , and vertical $\bar{w}$ velocity and their standard deviations of the red Vectrino co-located with WG7 at $x = 17.07 m$ for the LB test. . . . .	87

A.20 Mean cross-shore  $\bar{u}$ , alongshore  $\bar{v}$ , and vertical  $\bar{w}$  velocity and their standard deviations of the red Vectrino co-located with WG7 at  $x = 17.07\text{ m}$  for the LW test. . . . . 88

## LIST OF FIGURES

2.1	Schematic view of the high bare dune test including wave paddle, sandy beach profile on top of plywood slope, collection basin including sediment trap, water recirculation system, laser line scanner mounted to a motorized cart and location of the instruments measuring the hydrodynamics. . . . .	6
2.2	Equipment for measuring overtopped water and overwashed sediment volumes including the collection basin, sediment trap, and WG9. . .	8
2.3	Sediment trap before a wave run (left) and during an overwash event (right). . . . .	9
2.4	Schematic illustration of the initial profile geometry of the high (left) and low (right) dune test series. . . . .	10
2.5	Parameters of the chosen dowels modeling vegetation including its diameter $d_d$ , spacing $s$ , and its length divided into the burial depth $l_b$ and emerged height $l_e$ . . . . .	12
2.6	Vegetation configurations for the HN (left), HW (middle), and LW (right) test under initial conditions. The HW and LW tests show the same setup of the vegetation field. . . . .	13
2.7	Schematic top view of the dowel field showing a uniform spacing in all directions and its corresponding area of $A_v$ . . . . .	13
2.8	Template to create a uniform vegetation field throughout the experiment. . . . .	14
2.9	Vectrino Probe (Nortek, 2009). . . . .	19
3.1	Cross-shore variations of mean (top) and standard deviation (middle) of free surface elevation $\eta$ and wet probability $P_w$ (bottom) for HB (left), HN (middle), and HW (right) tests. . . . .	28

3.2	Cross-shore variations of mean (top) and standard deviation (bottom) of free surface elevation $\eta$ for LB (left), and LW (right) tests. . . . .	29
3.3	Temporal variations of the mean (top) and standard deviation (bottom) of the cross-shore velocity at the three velocimeters during the HB (left), HN (middle), and HW (right) tests. . . . .	41
3.4	Temporal variations of the mean (top) and standard deviation (bottom) of the cross-shore velocity at the three velocimeters during the LB (left), and LW (right) tests. . . . .	42
3.5	Temporal variations of wave overtopping rate $q_o$ (top), sand overwash rate $q_{bs}$ (middle), and ratio $q_{bs}/q_o$ (bottom) for the high dune test series. . . . .	50
3.6	Temporal variations of wave overtopping rate $q_o$ (top), sand overwash rate $q_{bs}$ (middle), and ratio $q_{bs}/q_o$ (bottom) for the low dune test series. . . . .	51
3.7	Dune profile evolution for HB (top), HN (middle), and HW (bottom) tests. The color scale from red (initial profile) to blue (final profile) indicates the measured profile number (HB, HN: 1 – 6; HW: 1 – 28) and the corresponding time level (HB, HN: 0 – 2, 400 s; HW: 0 – 11, 200 s). . . . .	57
3.8	Dune profile evolution for LB (top), and LW (bottom) tests. The color scale from red (initial profile) to blue (final profile) indicates the measured profile number (LB: 1 – 3; LW: 1 – 20) and the corresponding time level (LB: 0 – 1, 200 s; LW: 0 – 8, 000 s). . . . .	58
3.9	Photos taken during the HW (left and middle) and LW (right) tests illustrating scarping and slumping processes for the high dune test series and the hump formed during the low dune test with the wide vegetation. . . . .	58
3.10	Temporal variations of cumulative sand volume change $V_c$ (top), and overwash volume $V_o$ (bottom) per unit width for HB, HN, and HW tests. . . . .	65
3.11	Temporal variations of cumulative sand volume change $V_c$ (top), and overwash volume $V_o$ (bottom) per unit width for LB, and LW tests. . . . .	66

## ABSTRACT

The observed increase of population in coastal areas worldwide and the rise in sea level highlight the importance of protecting the coast. It is commonly known that a beach with a dune provides storm protection. However, rapid profile changes and destruction of sand dunes may be caused by wave-induced overwash and increase the flood risk landward of the dunes. This investigation examines a possible non-intrusive form of shore protection. Vegetation has been used to stabilize dunes against wind and wave attenuation by vegetation has been investigated to predict wind waves propagating across inundated vegetated areas. However, the effects of vegetation on dune erosion and overwash during storm events has never been studied.

A laboratory experiment encompassing five tests on the effects of woody plants on erosion and overwash of high and low dunes was performed. While foredune scarping occurred for the three high dune tests, it did not occur for the two low dune tests. In comparison to the respective bare dune, wave overtopping and overwash was not reduced by a narrow vegetation zone on a steep backdune of a high dune. However, a wide vegetation zone covering the high dune reduced foredune scarping, prevented wave overtopping initially and reduced sand overwash after the initiation of wave overtopping. By retarding wave uprush and reducing wave overtopping and overwash, a wide vegetation zone covering an entire low dune reduced dune erosion.

The data set obtained will be applied in future to extend the time-and depth averaged, process based numerical model CSHORE to include the vegetation effects on wave overtopping and overwash of vegetated dunes. The extended CSHORE may be applied to prototype dunes.



## Chapter 1

### INTRODUCTION

The accelerated population growth in coastal areas is occurring worldwide. 44% of the world's population live less than 150 *km* away from the coast (United Nations Atlas of the Oceans). According to Crowell et al. (2010), 8,651,000 people in the U.S., which is slightly more than 3% of the U.S. population, live in areas subjected to the 1% annual chance (100 year) coastal flood. Therefore, the vulnerability of coastal areas is characterized by a high density of human habitation and tourist infrastructure. These trends emphasize the importance of the coastline storm protection. Additionally, the risk is intensified by sea level rise. Gutierrez et al. (2007) point out that shoreline erosion and dune overwash will be increased by mean sea level rise. In many coastal areas, dunes (natural and artificial) play an important role of coastal protection. Tropical and extra-tropical storms, however, can lead to major coastal overwash events that cause serious damage to the coastal infrastructure.

Leatherman (1981) defines overwash as the flow of water and sediment across the crest of a beach or dune that does not directly return to the water body it originated from. According to Augustin et al. (2009), researchers are looking for solutions to reduce the severity of dune overwash and flooding. Recently coastal engineers are eager to pursue more non-intrusive forms of shore protection. Vegetation may be one solution for this new path. It protects the shoreline and provides a natural habitat for many different species. Vegetation supports shoreline protection by dampening incoming waves and depositing sediment in vegetated regions. An important parameter in storm wave and surge models is the bottom roughness coefficient associated with wave energy dissipation. Studies to quantify wave friction factors due to vegetation are very limited. Stem geometry, density, spatial coverage, buoyancy, and stiffness

are plant characteristics related to wave attenuation by emergent and submerged vegetation along with hydrodynamic parameters such as water depth, wave period and height.

Investigations of dune overwash have been mostly based on field observations before and after storm events. The storm impact and short-term poststorm recovery along a 200-km stretch due to Hurricane Ivan were investigated by Wang et al. (2006) by comparing one prestorm and three poststorm beach profile surveys. Judge et al. (2003) examined existing indicators of dune erosion vulnerability and described the development of a new parameter to characterize dune vulnerability to storm-induced erosion. The field data lead to a better qualitative understanding of dune overwash events. However, the progression of dune erosion and overwash during a storm event remains uncertain. Figlus et al. (2009) conducted laboratory experiments encompassing three different dune geometries to investigate the transition from minor to major overwash of dunes. The study included the measurement of the dune profile evolution. Presently no accepted similitude exists for coastal sediment transport in laboratory and field conditions.

Vegetation has been applied to stabilize dunes against aeolian transport. However, the effect of vegetation on overwash has been discussed but has never been measured as pointed out by Donnelly et al. (2006). Active planting of vegetation is suggested by Rosati and Stone (2009) as one possible countermeasure to reduce the severity of dune overwash and flooding. Wave attenuation by vegetation has been investigated to predict wind waves propagating across inundated vegetated areas. Dean and Bender (2006) analyzed static wave setup with emphasize on the effects of wave dampening by vegetation and bottom friction. Wave diffraction due to localized areas of wave energy dissipation, such as dense stands of kelp, pile clusters, or submerged trees was examined by Dalrymple et al. (1984). The wave-induced flow field in areas of fixed and flexible vegetation was investigated by Asano et al. (1992), Kobayashi et al. (1993), and Méndez et al. (1999). Asano et al. (1992) presented an analytical solution for water waves propagating over submerged swaying vegetation. Asano

(2008) analyzed tsunami attenuation in coastal forests. Algera (2006) described the usage of vetiver grass in tropical regions to stabilize soil structures and arable land. Flow velocities are reduced and soil is retained due to the stiff grass stems and firm roots. An example was given of a dike in Vietnam where vetiver grass was planted. A crest height reduction of 90 *cm* was estimated for a combination of two vetiver grass hedges. Furthermore, Bender et al. (2008) and Augustin et al. (2009) investigated numerically and experimentally the effect of coastal marshes on nearshore waves after Hurricane Katerina in 2005. The effect of coastal marshes was also studied by Resio and Westerink (2008). A laboratory study was conducted by Løvås and Tørum (2001) to investigate water propagation above a submerged vegetation in the surf zone and the effect of the submerged vegetation on dune erosion. The kelp caused significant wave attenuation but did not reduce dune erosion.

The Notsukezaki Sand Spit, which is located in the eastern Hokkaido, is the largest sand spit in Japan and its erosion problem has persisted since the 1960s. A low dune on the seaward side of the spit is covered with woody plants. The analysis by Hayashi et al. (2010) of the collected data including bathymetric information obtained in October 2004 and July 2007 indicated that the woody plants on the dune crest and backdune may have prevented dune overwash.

This study is based on a laboratory experiment conducted in a wave flume to gain information about the effects of vegetation on dune erosion. The profile evolution was measured of bare and vegetated dunes in the presence of wave overtopping and overwash. Woody plants were simulated by cylindrical wooden dowels that may reduce overtopping flow more than grass. Two different dune profiles were tested, high and low dunes. For the high dune test series bare, narrow vegetated, and wide vegetated dunes were tested, whereas for the low dune test series bare and wide vegetated dunes were examined. The narrow vegetation had only minor effect on the dune profile evolution. However, the wide vegetation on the foredune and backdune reduced scarping and slumping on the foredune. In the following, the experimental setup is described and an overview of the data analysis is given. The analyzed data are examined to evaluate

the effects of vegetation on wave overtopping and overwash as well as dune profile evolution.

## Chapter 2

### EXPERIMENT

This chapter provides an overview of the laboratory setup of the experiment conducted in the University of Delaware (UD) wave flume. Continuous measurements included free-surface elevation via capacitance wave gauges and fluid velocity via Acoustic Doppler Velocimeters. Besides hydrodynamics, special focus was placed on measuring accurate bottom elevation as well as water overtopping and sediment overwash data. For monitoring the evolving bottom morphology at high resolution in time and space, three-dimensional laser scans were performed by a laser line scanner system. A collection basin including a sediment trap was installed to measure water and sediment volumes transported over the dune. Wooden dowels were planted in three of the five tests conducted to examine the effects of vegetation on dune erosion. First, the experimental setup is described in general before more detailed information is given on the test procedure, the instruments for the hydrodynamic measurements, and the vegetation model and arrangement.

#### 2.1 Experimental Setup

The UD wave flume used in the experiment is 30 *m* long, 2.5 *m* wide, and 1.5 *m* high. Wooden boards were placed in the centerline of the flume to divide the flume into two sections in longshore direction. The division provided a reduction in the necessary amount of fine sand and water level change due to wave overtopping. Furthermore, it minimized seiching in the flume. The experimental setup, which is similar to the setup used during the dune overwash experiment by Figlus et al. (2009), is illustrated in Figure 2.1.

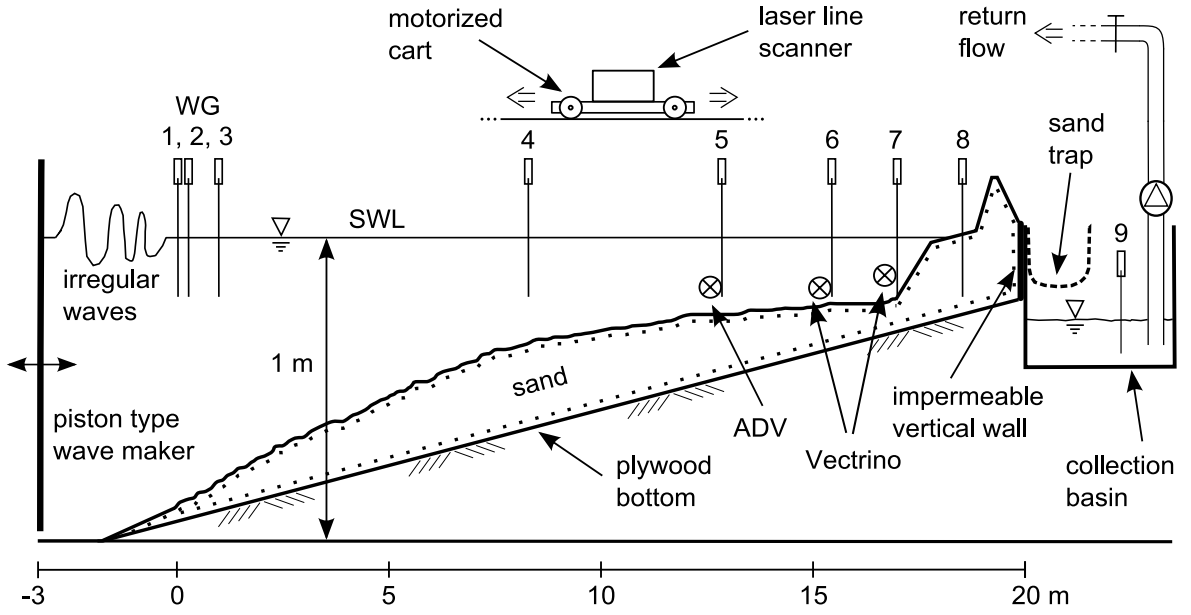


**Figure 2.1:** Schematic view of the high bare dune test including wave paddle, sandy beach profile on top of plywood slope, collection basin including sediment trap, water recirculation system, laser line scanner mounted to a motorized cart and location of the instruments measuring the hydrodynamics.

A  $400 - s$  irregular wave train with a TMA spectral shape was generated by the paddle of the piston-type wave maker located at the offshore end of the flume in a water depth of  $1\text{ m}$ . At the opposite end of the wave maker a gravel beach was built to absorb wave energy. The sand beach was placed on top of a  $1 : 30$  rigid sloping plywood bottom starting approximately  $3\text{ m}$  from the wave paddle to the impermeable vertical wall at the onshore end of the flume section used for this experiment. The fine sand placed in the wave flume could be regarded as coarse sand at prototype scale. Buck et al. (2007) determined the median diameter  $d_{50}$ , specific gravity  $s = \rho_s/\rho_w$ , porosity  $n_p$  and fall velocity  $w_f$  of the fine sand. A summary of the well-sorted fine sand's parameters is given in Table 2.1. The grain size distribution was given in Figlus et al. (2009). To measure the hydrodynamics during each  $400 - s$  wave burst, eight capacitance wave gauges (WG) recorded the free surface elevation. The fluid velocity was measured by three acoustic Doppler velocimeter sensors (one 2D ADV and two

Vectrinos).

**Table 2.1:** Sediment characteristics.

color	light brown
grain shape	subangular to subrounded
USCS label	SP (poorly graded sand)
$d_{16}, d_{50}, d_{84}$	0.124 mm, 0.183 mm, 0.221 mm
$d_{10}, d_{30}, d_{60}$	0.117 mm, 0.146 mm, 0.194 mm
$s, n_p, w_f$	2.6, 0.4, 2.0 cm/s

The main addition to the flume for the overwash experiments conducted by Figlus et al. (2009) was the equipment to collect the overtopped water and sediment in a water collection basin behind the vertical wall on an acceptable level of accuracy (Figures 2.2 and 2.3). With its dimension of 2.44 m x 0.97 m x 0.78 m, the rectangular basin has a capacity of 500 gallons (1900 liters). In addition to a mechanical float gauge, an electronic capacitance wave gauge (WG9) was installed to read the water level in the basin. A sand trap was located inside the water collection basin to measure the temporal variations of overwash transport rates. The trap was constructed of a lightweight aluminum frame and a woven nylon fabric mesh with a micron rating of 74 retaining particles larger than 74  $\mu\text{m}$  (silt: 4 – 62.5  $\mu\text{m}$ ). It was important to maintain a constant water level in the flume during each run. Whenever a water level drop of 1 mm occurred in the flume, a recirculation system pumped the collected water out of the basin back into the flume. An inline flow meter (FM) capable of measuring fluid velocities between 0.3 and 10 m/s was installed to measure the water volume pumped back into the flume.

For this experiment it was crucial to obtain measurements of profile changes at high spatial and temporal resolution. A state-of-the-art profiling system was installed in the flume to obtain accurate profile data after the water level was lowered. It consisted of a class III. *Acuity AR4000 – LIR* laser line scanner system in conjunction with a class II. *Acuity AR1000* laser distance finder. The laser system works only in

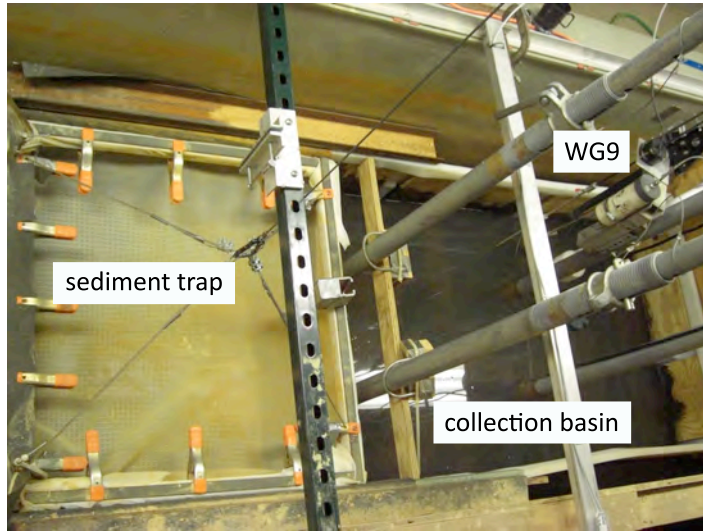


**Figure 2.2:** Equipment for measuring overtopped water and overwashed sediment volumes including the collection basin, sediment trap, and WG9.

air. In an effort to automate the profile measurements, the laser line scanner system was mounted on a cart controlled by a servo motor with continuously adjustable speed setting of up to  $10\text{ cm/s}$ . This set up allowed movement of the laser line scanner back and forth along the flume's cross-shore ( $x$ ) axis on a set of T-tracks. Its horizontal laser beam deflected by a rotating mirror assembly prescribed a  $360^\circ$  sweep in the vertical ( $y - z$  coordinate) plane normal to the cross-shore coordinate  $x$ . Up to 50,000 distance samples per second could be recorded. To obtain information on the cross-shore coordinate  $x$  of the  $2D$  slice scanned at any point along the flume, a laser distance finder was installed next to the collection basin at the height of the motorized cart. By using a reflective target, distances up to  $150\text{ m}$  could be measured with an accuracy of  $\pm 2\text{ mm}$  by the *AR1000* sensor during movement of the cart at a constant speed of  $1\text{ cm/s}$  (Acuity, 2003). The synchronized distance data achieved from the two lasers allowed the recreation of the 3D flume topography. More detailed information on the laser instruments and the profile measurement method were given in Figlus et al. (2009). Compared to rapid changes in the bottom profile in the region of the dune, changes offshore were minor and it was sufficient to measure the offshore part of the



**Figure 2.3:** Sediment trap before a wave run (left) and during an overwash event (right).

profile with an array of three ultrasonic thickness gauges. The three transducers were mounted 30 *cm* apart from each other on a specialized vernier caliper attached to a cart that was moved manually. This method recorded submerged profile data less precisely than the laser line scanner but reduced the water level lowering to measure the entire beach profile.

## 2.2 Test Overview

The five tests conducted are explained in the following.

### 2.2.1 Tested Nearshore Profiles

Two different dune profiles were tested in this study with the denotations of high (H) and low (L) dunes. The initial profiles are depicted in Figure 2.4. The high dune with its crest elevation of 21 *cm* above the still water level (*SWL*) is illustrated in the left panel. Its geometry shows fairly steep foredune and backdune slopes of 1/2 and 1/3, respectively, whereas the slopes of the low dune (right panel) are gentler. The foredune and backdune slopes were 1/6 and 1/12, respectively. Additionally, the berm slope of the low dune was 1/16 and submerged in comparison to the partially emerged 1/30 slope of the high dune. However, the bottom profiles seaward of the berm were

fairly similar. The geometry of the high dune was chosen to be the same as for the BD (dune with berm) test performed by Figlus et al. (2009). The offshore beach profile was somewhat different from that of the BD test due to the cumulative wave action in the subsequent experiments since 2009.

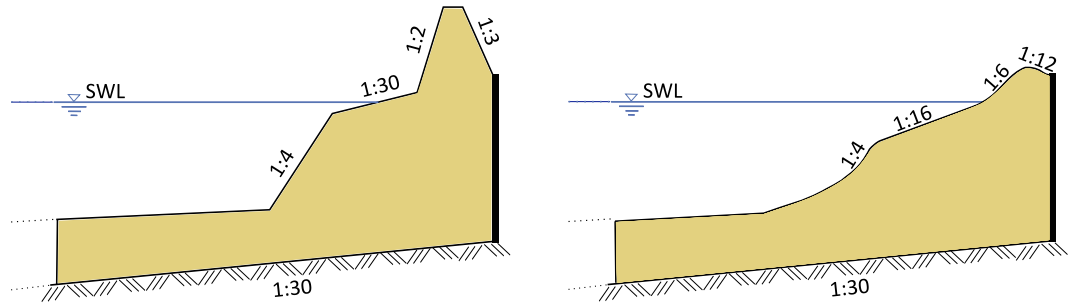


**Figure 2.4:** Schematic illustration of the initial profile geometry of the high (left) and low (right) dune test series.

The five tests in Table 2.2 were conducted in sequence. In addition to the notations, the table includes the total duration of each test which comprised a number of runs of the same 400 – s bursts of irregular waves impinging on the dune. The high and bare (HB) dune test was terminated after 6 runs (2,400 s) when the dune crest was lowered to the elevation of the wall crest. To maintain the same initial profile under the presence of two different vegetation configurations, the high dune geometry was reconstructed for narrow (HN) and wide (HW) vegetation tests. The narrowly vegetated high dune was eroded to the level of the wall crest after 6 runs as was the case with the HB test. The wide vegetated high dune was more resilient. The HW test was terminated after 28 runs (11,200 s) due to alongshore variability of the scarped dune profile. After the last run of the HW test, the dowels were removed. Subsequently, the scarped dune profile was smoothed out to an alongshore uniform profile which was then used as the initial profile for the low and bare dune (LB) test. It took 3 runs (1,200 s) to erode the dune for the LB test up to the vertical wall. After rebuilding the low dune profile, 20 runs (8,000 s) were generated to examine the temporal variations

of the wave overtopping and the sediment overwash rate after the vertical wall was exposed to wave action. The water level in front of the wave maker was 1.00 *m* for all five tests. The vegetation model and configurations are explained in the next chapter.

**Table 2.2:** Test overview and notations.

Test	Dune	Vegetation	Water depth (m)	Number of runs	Total duration (s)
HB	High	Bare	1.0	6	2,400
HN	High	Narrow	1.0	6	2,400
HW	High	Wide	1.0	28	11,200
LB	Low	Bare	1.0	3	1,200
LW	Low	Wide	1.0	20	8,000

### 2.2.2 Vegetation Modeling

The focus of this study is the effect of vegetation on dune erosion. Rigid woody plants instead of grass were selected and simulated by cylindrical wooden dowels. Branches and leaves were not included for simplicity. The resistance to the overtopping flow and the reduction in wave overtopping was expected. The vegetation effects on the dune profile evolution may be separated into flow resistance and sand reinforcement attributable to the exposed and buried parts of the dowels, respectively. The sand reinforcement effect was uncertain for lack of data.

Figure 2.5 illustrates the chosen dowels with a diameter of  $d_d = 0.9$  *cm* and a total length of 30 *cm*. The burial depth of  $l_b = 20$  *cm* and the emerged height of  $l_e = 10$  *cm* were chosen in this experiment of no uprooting. The dowels were placed in the region of rapid profile changes, therefore the burial depth was adjusted to 20 *cm* after each 400 – *s* wave burst. In this experiment the dowels were mostly in the swash zone and were not completely submerged due to the 10 *cm* height above the sand bottom. A uniform spacing of  $s = 4$  *cm* among the dowels was chosen for all vegetation tests in this exploratory experiment.

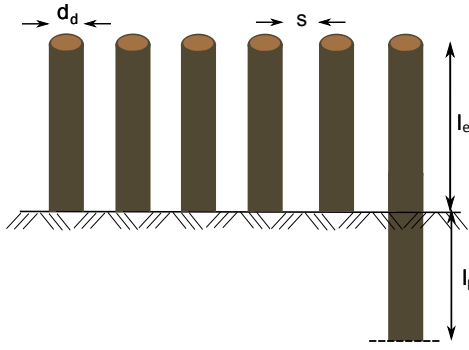


**Figure 2.5:** Parameters of the chosen dowels modeling vegetation including its diameter  $d_d$ , spacing  $s$ , and its length divided into the burial depth  $l_b$  and emerged height  $l_e$ .

The flume section used for this experiment as described in Chapter 2.1 was 1.15 m wide. Wooden templates were used to build the same initial dune profile. Each template had a width of 2 cm and the effective width of the sand profile in the dune zone was 1.11 m. The narrow vegetation extended from the vertical wall at  $x = 19.90$  m to the cross-shore location of  $x = 19.50$  m close to dune crest. The 40 cm ( $x = 19.50 - 19.90$  m) stretch of the backdune was covered with 10 rows with each row consisting of 28 dowels as shown for the HN test in Figure 2.6. That leads to a stem density of  $N = 0.063/cm^2$  where  $N = \text{number of stems/area}$ . In addition to the backdune, the wide vegetation also covered the fordune in the zone of  $x = 19.10 - 19.90$  m. With the same spacing of  $s = 4$  cm, the configuration of the wide vegetation consisted of 20 rows of the dowels over a 80 cm cross-shore stretch of the dune profile as shown for the HW and LW tests in Figure 2.6. Due to the equal spacing, the stem density remained the same for both cases. All three pictures were taken on the initial dune profile with the vegetation before the exposure to wave action.

Scanning the vegetated dune zone was found to be challenging. Laser measurements at a cross-shore interval of 1 cm instead of 2 cm used in the zone of no vegetation allowed the profile measurement among the dowels spaced at the 4 cm intervals as discussed in Chapter 3.2.2. A schematic drawing of the dowel field set up is illustrated in Figure 2.7 which shows the uniform spacing of  $s = 4$  cm and its corresponding area of

$A_v = 16 \text{ cm}^2$  for each dowel.



**Figure 2.6:** Vegetation configurations for the HN (left), HW (middle), and LW (right) test under initial conditions. The HW and LW tests show the same setup of the vegetation field.

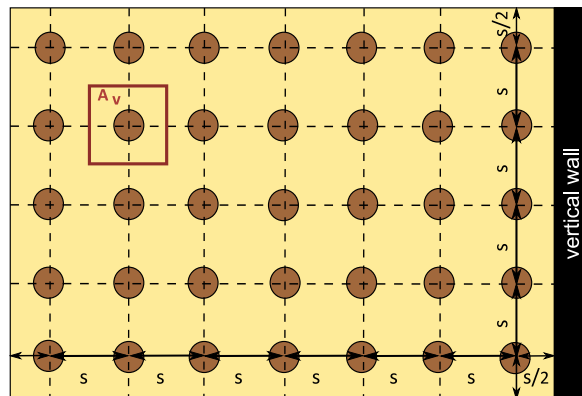


**Figure 2.7:** Schematic top view of the dowel field showing a uniform spacing in all directions and its corresponding area of  $A_v$ .

To ensure uniform and equal spacings of the dowels throughout the experiment, a template was created out of a hard but flexible cardboard. The template could be removed easily after the dowels were buried into the sand. The photo in Figure 2.8 was taken during the process of creating a vegetation field.



**Figure 2.8:** Template to create a uniform vegetation field throughout the experiment.

### 2.3 Test Procedure

The test procedure consisted of several steps and is the same for all tests performed. First, the initial beach profile was constructed which was followed by a measurement of the entire beach profile. Two different measurement systems were employed to record the bottom morphology. While high resolution 3D scans of the subaerial portion of the bed profile ( $x = 4.90 - 19.90 \text{ m}$ ) were delivered by the laser line system, an array of three submerged ultrasonic transducers was applied for the submerged portion ( $x = 0 - 5.9 \text{ m}$ ). The overlapping of  $1 \text{ m}$  ensured an accurate combination of both profile measurement methods. The wooden dowels were placed for the HN, HW, and LW tests. Subsequently, the instruments measuring the hydrodynamics during each  $400 - s$  wave burst were installed in the flume. The three landward wave gauges were attached to bars that were mounted to the side walls of the flume section because they did not need to be removed for the laser scan measurements throughout the experiment. As explained in the next Chapter 2.3.1, the landward gauges were buried in the sand when they were situated in the swash zone. The other five wave gauges and the velocimeters were fixed to the carts or bars on the tracks and had to be removed before each profile measurement.

To convert voltages recorded by the wave gauges into water level values for the

data analysis, all gauges were calibrated on the day of the measurement. An automated procedure was applied to obtain a calibration curve for each of the eight gauges. Since passing waves represent a positive free surface elevation above *SWL*, the first step of the daily calibration consisted of raising the water level in the flume above *SWL*, which was limited by the dune crest height to avoid water overflowing over the dune. A motorized wave gauge located offshore close to WG3 was used as a reference gauge for this calibration method. Before the actual automated calibration of the eight wave gauges, the reference wave gauge was lowered into the water via a stepper motor while recording voltage values at an interval of 1 *cm*. For the automated daily calibration all eight wave gauges recorded the voltages for every 1 *cm* of water level change detected by the reference gauge while draining the flume. The buried wave gauge (WG8) however, was calibrated before its burial into the beach sand because the submerged segment of WG8 located on the berm was not long enough for the above described calibration method. During the manual calibration of WG8, the wave gauge was emerged step by step into a cylindrical container filled with water. It was calibrated for a range of  $\pm 15$  *cm* around its center at the same interval of 1 *cm*. The other two buried wave gauges (WG6 and WG7) could be calibrated in the same way as WG1-WG5 because of the sufficient submerged lengths. Further explanation follows in the next Chapter [2.3.1](#). Gauge WG9 was used to measure the water level in the collection basin and was not included in the daily calibration. Thus, it had to be calibrated daily separately from the other gauges. Since it was also motorized, its calibration was the same as the reference gauge calibration.

After the completion of the calibrations, a still water level (*SWL*) reading of all wave gauges was taken to obtain the reference datum corresponding to *SWL* for the determination of the free-surface elevation. Furthermore, the exposed wire length and water depth at each buried wave gauge was recorded. In case of wave overtopping the water level at WG9 located in the collection basin was recorded for 10 *s* after each run to obtain the water volume change in the collection basin. The input signal sent to the wave maker consisted of a time series of voltage values corresponding to a certain paddle

displacement aiming to reproduce an irregular wave train with a TMA spectral shape over a duration of 400 *s*. The spectral significant wave height and spectral peak period were approximately  $H_{mo} = 19 \text{ cm}$  and  $T_p = 2.6 \text{ s}$ , respectively. A National Instruments 16 channel SCSI data acquisition board recorded the data of all instruments during each run at the same frequency of 20 *Hz* as the input signal sent to the wave maker. An user interface by LabView was used to control the acquisition board, handle data logging, and control the wave maker.

The collection basin and the sand trap behind the vertical wall allowed for measuring the cumulative water overtopping and sand overwash volumes during each run. The sand trap was emptied after each single run. After obtaining the wet weight of the sand, the wet sand was dried in an oven for 24 *hours* and the dry sand weight was measured. The water level change in the collection basin was obtained using WG9 and a mechanical float gauge. For the case of minor overwash a small tub was placed in the basin underneath the sediment trap to measure the small water volume more accurately. The wave overtopping volume was the sum of the pumped volume, the volume change in the basin or tub, and the water volume in the wet sand.

To examine the evolution of the bottom profile in this experiment, profile measurements were taken whenever the profile change was noticeable. The laser line scanner was mounted on a motorized cart that moved along the wave flume while taking profile measurements. This necessitated clearance of the instruments blocking the track of the cart. Besides the laser distance finder based on a time-of-flight measurement of the emitted laser beam reflecting from a target, the laser line scanner system is based on time-of-flight in air as well. Each profile measurement required lowering the water level in the flume. In contrast to the most prominent changes in the region between  $x = 16.0 - 19.9 \text{ m}$ , changes offshore were minor and it was sufficient to employ three 1 *MHz* ultrasonic transducers connected to a Panametrics 25*MX* precision thickness gauge via a *MX* – 8 multiplexer. Their utilization allowed the profile measurements under water since the zone between  $x = 0 - 6 \text{ m}$  did not need to be drained. The transducers obtain water depth at a specific location by converting the time for acoustic

signals to be reflected from the sandy bottom. While laser recordings were automated, the vernier caliper was mounted to an unmotorized cart. To guarantee the distance measurement within acoustic signal accuracy, the vernier caliper was adjusted before each recording. Readings were taken at 10 *cm* cross-shore intervals.

### 2.3.1 Wave Gauges

Eight single-wire capacitance wave gauges (WG) were installed along the centerline of the flume. Starting offshore, the gauges are numbered WG1 through WG8 as shown in Figure 2.1. Table 2.3 lists the specific location of each of the eight wave gauges. Wave gauges WG1, WG2 and WG3 situated outside of the surf zone were used to separate incident and reflected waves as well as to monitor the repeatability of wave runs in each test. The chosen spacing of the three wave gauges WG1, WG2, and WG3 yields a resolvable frequency range of 0.15 – 1.70 *Hz* for the separation of incident and reflected waves using linear wave theory. The transformation of the shoaling and breaking wave train was recorded by WG4 to WG8. Most of the irregular wave breaking occurred from WG4 to WG5. WG6 and WG7 measured the free surface elevations in the inner surf zone, whereas WG8 was located in the swash zone of wave uprush and downrush on the berm. In contrast to the free wave gauges (WG1-WG5) located further offshore, the experimental setup required to bury WG6 and WG7 slightly in the sand and WG8 deep into the sand in order to avoid the exposure of the gauge tip in air. WG8 recorded the wet sand surface when the sand surface was exposed to air. The resulting classification of all wave gauges is presented in Table 2.3. The analysis of the recorded data of the exposed WG8 will be explained in Chapter 3.1.2.

**Table 2.3:** Location and classification of all wave gauges for all five tests.

	<b>WG1</b>	<b>WG2</b>	<b>WG3</b>	<b>WG4</b>	<b>WG5</b>	<b>WG6</b>	<b>WG7</b>	<b>WG8</b>
<b>x(m)</b>	0.00	0.25	0.95	8.30	12.90	15.52	17.07	18.61
<b>free</b>	✓	✓	✓	✓	✓	✓	✓	–
<b>buried</b>	–	–	–	–	–	–	–	✓
<b>submerged</b>	✓	✓	✓	✓	✓	✓	✓	–
<b>exposed</b>	–	–	–	–	–	–	–	✓

### 2.3.2 Velocity Measurements

The experimental setup in Figure 2.1 included three instruments that measured the fluid velocity continuously during each wave run. In addition to a 2D Acoustic Doppler Velocimeter (ADV) with a sideward facing probe by SonTek, two Vectrinos by Nortek were employed. The 2D ADV recorded the fluid velocity in cross-shore ( $u$ ) and alongshore ( $v$ ) direction, whereas the two Vectrinos register vertical velocity ( $w$ ) as well. It is noted that the measured alongshore and vertical velocities were small in comparison to the cross-shore velocities in this experiment. The measuring volumes of all velocimeters were each positioned at  $2/3$  of the local water depth  $d$  below  $SWL$  at the beginning of each run. Fine suspended sand affected the fluctuating velocity components and the estimated error was  $\pm 0.5$  cm/s. Table 2.4 lists the location of the measurement probe of the three velocimeters at the cross-shore locations of WG5-WG7 during the entire experiment. The velocimeters were placed off the centerline of the flume.

The Vectrino by Nortek shown in Figure 2.9 is a versatile, high-precision instrument that uses acoustic sensing techniques to measure flow in a remote sampling volume without disturbing it. It is a high-resolution acoustic velocimeter developed primarily for laboratory measurements. Its measurement technology is based on coherent Doppler processing, which is characterized by accurate data with no appreciable zero offset (Rusello, 2009). All electronics are included in the base instrument. Components

**Table 2.4:** Location of all three velocimeters for all five tests.

	<b>2D ADV at WG5</b>	<b>Vectrino Blue at WG6</b>	<b>Vectrino Red at WG7</b>
$x (m)$	12.90	15.52	17.07
$y (m)$	0.19	0.14	0.08
$z (m)$	$-2/3 d$	$-2/3 d$	$-2/3 d$

*d = local water depth at the start of each run.*

of the Vectrino are four transducers/receivers and a side looking probe (comparable to the 2D ADV) which improves turbulence measurements and provides redundancy. The reduced size of the probe, which includes a temperature sensor, minimizes the flow interference from the probe itself. Furthermore, noise is reduced by the increased internal sampling rate. Data collection is possible up to a frequency of 200  $Hz$ . (Nortek, 2009)



**Figure 2.9:** Vectrino Probe (Nortek, 2009).

## Chapter 3

### DATA ANALYSIS

In this chapter a detailed description of the data analysis is presented. The collected data is organized into three main categories: hydrodynamics, overtopping and overwash rates, and morphological evolution. The following variables are presented to examine the effects of vegetation on wave overtopping and overwash processes:

$$\underbrace{\bar{\eta}, \sigma_{\eta}, P_w}_{\text{free surface elevation}} \quad \underbrace{\bar{u}, \sigma_u}_{\text{fluid velocity}} \quad \underbrace{q_{bs}, q_o}_{\text{overwash}} \quad \underbrace{z_b}_{\text{profile elevation}}$$

where time averaged values are indicated by an overbar. The eight wave gauges and three velocimeters in the experiment are analyzed to obtain the statistical values of the hydrodynamics including the mean free surface elevation  $\bar{\eta}$ , the corresponding standard deviation  $\sigma_{\eta}$  and wet probability  $P_w$ , the mean cross-shore velocity  $\bar{u}$  and its standard deviation  $\sigma_u$ . The data from the sediment trap and the collection basin installed in the flume are analyzed to obtain the sediment transport rate  $q_{bs}$  and water overtopping rate  $q_o$ . The profile elevation  $z_b$  is found by analyzing the laser and acoustic measurements.

#### 3.1 Hydrodynamics

The data from the eight single-wire capacitance wire wave gauges (WG1-WG8) placed along the centerline of the wave flume are used to examine the transformation of the shoaling waves from offshore through steepening and breaking all the way to the creation of uprush and overwash events. The specific location of each wave gauge and velocimeter is listed in Tables 2.3 and 2.4 in Chapter 2.3. In the following chapters, all statistical values are based on the last 380 s of each run consisting of about 200

waves. The first 20 s of each 400 s time series are considered as ramp-up phase and not included in the statistical analysis.

### 3.1.1 Incident Wave Characteristics

The three wave gauges (WG1, WG2 and WG3) located offshore in Figure 2.1 are employed to separate incident and reflected waves at the location of WG1. The incident wave parameters are represented by the spectral significant wave height  $H_{mo}$ , the root-mean-square wave height  $H_{rms}$  and the significant wave height  $H_s$  as well as by the spectral peak period  $T_p$  and the significant wave period  $T_s$ . The spectral and time series parameters for each of the five tests are listed in Table 3.1 to 3.5. In addition, the reflection coefficient  $R$ , which is defined as the ratio between the values of  $H_{mo}$  for the reflected and incident waves, is tabulated in the last column. The average value is calculated for each parameter and is listed at the bottom of each table. The measured total (incident plus reflected wave) wave characteristics at WG1 are analyzed in the same manners and presented in Table A.1 to A.5 in the Appendix. The effects of reflective waves at WG1 are found to be small.

All offshore wave parameters remained fairly constant throughout the experiment since  $SWL$  was kept constant at 1.0 m and the same signal for wave generation was used for each 400 – s wave burst. For the five tests the average values of  $H_{mo}$  and  $H_{rms}$  are 19.1 cm and 13.5 cm, respectively. The values of  $H_s$  and  $H_{mo}$  are close for all five tests. The averaged spectral peak period was  $T_p = 2.6$  s.  $T_s$  was slightly less than  $T_p$  and slightly more variable with an overall average value of  $T_s = 2.3$  s. The value of  $R$  decreased slightly with the decrease of the foredune slope and the destruction of the dune during each test. Its average value was  $R = 0.16$  for the HB and HN tests. The narrow vegetation on the backslope did not reduce the erosion process and therefore did not influence the reflection coefficient. For the HW test with wide vegetation the average of the reflection coefficient was  $R = 0.15$ . Furthermore,  $R = 0.11$  for the LW test in comparison to  $R = 0.22$  for the LB test. The wide vegetation may have caused wave energy dissipation because of the reduced value of  $R$  for the HW and LW tests.

**Table 3.1:** Incident wave characteristics at WG1 ( $x = 0$  m) for the 6 runs of the HB test.

Run	$H_{mo}$ (cm)	$H_{rms}$ (cm)	$H_s$ (cm)	$T_p$ (s)	$T_s$ (s)	$R$
HB1	18.46	13.06	17.97	2.57	2.25	0.16
HB2	18.79	13.29	18.42	2.70	2.27	0.17
HB3	18.59	13.15	18.26	2.70	2.27	0.17
HB4	18.66	13.19	18.41	2.70	2.29	0.17
HB5	18.63	13.17	18.41	2.70	2.26	0.17
HB6	18.56	13.12	18.36	2.57	2.28	0.15
Average	18.61	13.16	18.30	2.65	2.27	0.16

**Table 3.2:** Incident wave characteristics at WG1 ( $x = 0$  m) for the 6 runs of the HN test.

Run	$H_{mo}$ (cm)	$H_{rms}$ (cm)	$H_s$ (cm)	$T_p$ (s)	$T_s$ (s)	$R$
HN1	18.53	13.10	18.10	2.57	2.30	0.17
HN2	18.73	13.25	18.57	2.57	2.28	0.17
HN3	18.60	13.15	18.41	2.57	2.32	0.18
HN4	18.86	13.33	18.36	2.57	2.27	0.17
HN5	18.89	13.36	18.50	2.57	2.29	0.15
HN6	18.43	13.03	18.38	2.57	2.30	0.14
Average	18.67	13.20	18.39	2.57	2.29	0.16

**Table 3.3:** Incident wave characteristics at WG1 ( $x = 0$  m) for the 28 runs of the HW test.

Run	$H_{mo}$ (cm)	$H_{rms}$ (cm)	$H_s$ (cm)	$T_p$ (s)	$T_s$ (s)	$R$
HW1	18.33	12.96	18.39	2.57	2.32	0.16
HW2	18.49	13.08	18.22	2.57	2.30	0.17
HW3	18.59	13.14	18.22	2.57	2.32	0.16
HW4	18.46	13.05	18.22	2.57	2.30	0.16
HW5	18.52	13.10	18.16	2.57	2.32	0.16
HW6	18.45	13.05	18.17	2.57	2.29	0.16
HW7	18.53	13.10	18.24	2.57	2.28	0.16
HW8	18.55	13.12	18.38	2.57	2.27	0.15
HW9	18.57	13.13	18.40	2.57	2.30	0.15
HW10	18.56	13.12	18.41	2.57	2.29	0.15
HW11	18.69	13.22	18.70	2.57	2.32	0.15
HW12	18.75	13.26	18.65	2.57	2.29	0.15
HW13	18.84	13.32	18.62	2.57	2.30	0.14
HW14	18.84	13.12	18.65	2.57	2.31	0.15
HW15	18.52	13.09	18.40	2.57	2.29	0.15
HW16	18.71	13.23	18.72	2.57	2.26	0.14
HW17	18.71	13.23	18.48	2.57	2.26	0.14
HW18	18.33	12.96	18.25	2.57	2.29	0.14
HW19	18.52	13.10	18.43	2.57	2.27	0.14
HW20	18.61	13.16	18.40	2.57	2.30	0.14
HW21	18.49	13.07	18.29	2.57	2.28	0.14
HW22	18.57	13.13	18.41	2.57	2.28	0.14
HW23	18.53	13.10	18.55	2.57	2.28	0.14
HW24	18.14	12.82	17.86	2.57	2.30	0.14
HW25	18.32	12.95	18.10	2.57	2.30	0.14
HW26	18.44	13.04	18.39	2.57	2.30	0.14
HW27	18.29	12.94	17.94	2.57	2.29	0.13
HW28	18.23	12.89	18.00	2.57	2.31	0.13
Average	18.52	13.10	18.34	2.57	2.29	0.15

**Table 3.4:** Incident wave characteristics at WG1 ( $x = 0$  m) for the 3 runs of the LB test.

<b>Run</b>	<b><math>H_{mo}</math> (cm)</b>	<b><math>H_{rms}</math> (cm)</b>	<b><math>H_s</math> (cm)</b>	<b><math>T_p</math> (s)</b>	<b><math>T_s</math> (s)</b>	<b><math>R</math></b>
<b>LB1</b>	20.66	14.61	20.68	2.57	2.39	0.22
<b>LB2</b>	20.71	14.66	20.58	2.57	2.38	0.22
<b>LB3</b>	20.80	14.85	20.85	2.57	2.36	0.21
Average	20.80	14.71	20.70	2.57	2.38	0.22

**Table 3.5:** Incident wave characteristics at WG1 ( $x = 0$  m) for the 20 runs of the LW test.

Run	$H_{mo}$ (cm)	$H_{rms}$ (cm)	$H_s$ (cm)	$T_p$ (s)	$T_s$ (s)	$R$
LW1	18.24	12.90	17.97	2.57	2.28	0.12
LW2	20.13	14.24	19.70	2.57	2.29	0.12
LW3	20.17	14.26	20.00	2.57	2.29	0.11
LW4	21.15	14.96	21.08	2.57	2.35	0.21
LW5	18.20	12.87	17.93	2.57	2.32	0.10
LW6	18.46	13.05	18.24	2.57	2.38	0.10
LW7	18.54	13.11	18.38	2.57	2.33	0.10
LW8	18.54	13.11	18.38	2.57	2.33	0.10
LW9	18.81	13.30	18.64	2.57	2.31	0.10
LW10	18.92	13.38	18.67	2.57	2.33	0.10
LW11	19.19	13.57	18.81	2.57	2.32	0.11
LW12	18.79	13.29	18.58	2.57	2.31	0.10
LW13	17.84	12.62	17.64	2.57	2.35	0.10
LW14	18.94	13.39	18.76	2.57	2.33	0.10
LW15	18.74	13.25	18.50	2.57	2.33	0.10
LW16	18.70	13.22	18.52	2.57	2.34	0.11
LW17	18.76	13.27	18.58	2.57	2.32	0.10
LW18	18.78	13.28	18.60	2.57	2.32	0.11
LW19	19.03	13.46	18.95	2.57	2.33	0.11
LW20	19.10	13.40	18.74	2.57	2.32	0.11
Average	18.95	13.40	18.74	2.57	2.32	0.11

### 3.1.2 Free Surface Elevation and Wet Probability

The wave gauges measure the water free surface elevation ( $\eta$ ) during each wave run where the still water level ( $SWL$ ) serves as reference datum for all tests. Statistical properties including the mean free surface elevation ( $\bar{\eta}$ ), its standard deviation ( $\sigma_\eta$ ) and wet probability ( $P_w$ ) are computed for all eight wave gauges. The wet probability indicates the likelihood of a gauge to be submerged in water at any given time during the respective 400-s wave burst. It is calculated by dividing the points within the wet duration by the total number of data points. The free surface elevation ( $\eta$ ) is related to the bottom elevation ( $z_b$ ) and the time dependent local water depth where both the free surface elevation and the bottom elevation are in reference to the reference datum ( $z = 0$ ). This dependency is noticeable in particular for WG8 due to its placement in the berm. For some runs WG8 was located above  $SWL$  and was not always submerged throughout the entire run. To calculate the statistical values of  $\eta$ , only the wet data points are included in the analysis. The separation procedure of the wet and dry data points was explained in Figlus et al. (2009).

Table 3.6 to 3.16 list the free surface statistics for the five tests. WG1-WG3 were offshore outside the surf zone. WG4 was located near the breaker zone. WG5-WG7 were in the inner surf and WG8 was in the swash zone. Figures 3.1 and 3.2 summarize the cross-shore and temporal variations of the tabulated statistical values for the high and low dune test series, respectively. The upper panel of Figure 3.1 depicts  $\bar{\eta}$  with its standard deviation  $\sigma_\eta$  shown in the middle panel.  $P_w$  for all eight wave gauges is included in the bottom panel. All values are plotted as a function of  $x$  (m) where each circle represents each run at each wave gauge located at the given cross-shore location. Since the statistical parameters represent average values over the respective duration of 400 s, the circle is plotted at the middle of each run starting from  $t = 0$  at the beginning of each test. The temporal variation is shown by the color scheme ranging from red for the first run to the respective final run plotted in blue.

Figure 3.1 indicates a setdown ( $\bar{\eta} < 0$ ) for WG1-WG4 and a setup ( $\bar{\eta} > 0$ ) for the other wave gauges (WG4-WG8) located further onshore. Deviations from this trend for

a few runs in the LW test may be related to measurement or calibration errors. Overall,  $\bar{\eta}$  and  $\sigma_{\eta}$  show only minor variations over time except for the buried wave gauge WG8 affected by the rapid bottom elevation changes occurring at its location in comparison to small bottom changes in the zone between  $x = 0 - 17.1 m$ . For the high dune test series eroded sand from the dune was deposited in the berm region at the beginning of each test before the initiation of major overwash. This is why the value for  $\bar{\eta}$  shows an increase first before it continuously decreases due to the eroding bottom elevation. The standard deviation  $\sigma_{\eta}$  can be expressed by the spectral significant wave height,  $H_{mo} = 4\sigma_{\eta}$ , and  $\sigma_{\eta}$  decreases in the surf and swash zones. The values of  $\sigma_{\eta}$  at the location of WG8 increase during each test due to the berm erosion and lowering bottom elevation. The corresponding wet probability  $P_w$  for WG8 is listed in Table 3.16. All other wave gauges were submerged throughout the entire duration of the experiment and  $P_w = 1$  for WG1-WG7. On the other hand, WG8 was not continuously submerged during the first five runs of the HB and HN tests. Since the wide vegetation slowed down the erosion process, the shoreline at *SWL* was not located landward of WG8 until the end of HW7. Once WG8 was seaward of the still water shoreline, the wet probability became 1.0 and WG8 was wet always.

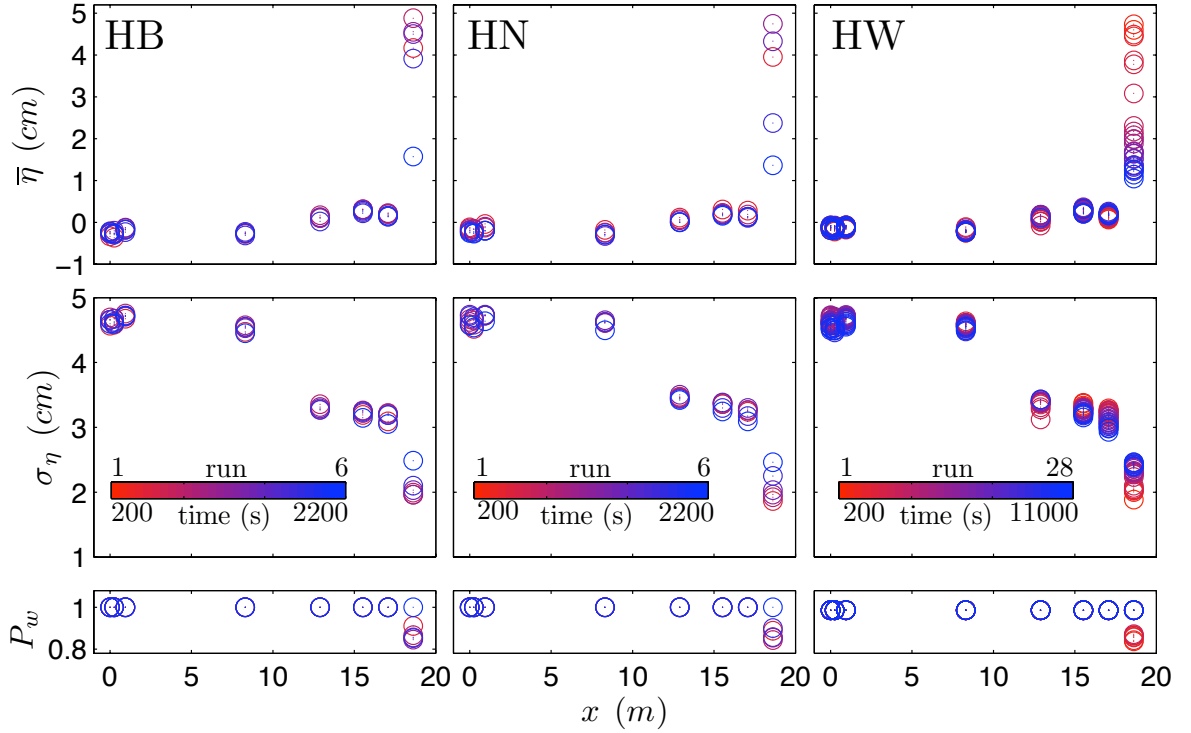


**Figure 3.1:** Cross-shore variations of mean (top) and standard deviation (middle) of free surface elevation  $\eta$  and wet probability  $P_w$  (bottom) for HB (left), HN (middle), and HW (right) tests.

Figure 3.2 shows similar cross-shore variations of  $\bar{\eta}$  and  $\sigma_\eta$  for the low dune tests to those depicted in Figure 3.1 for the high dune tests. This was expected since the incident wave conditions remained similar throughout the entire experiment. Furthermore, minor differences existed for the five tests in the bottom profile elevation between  $x = 0 - 17.1$  m. The overall decrease of  $\bar{\eta}$  and increase in  $\sigma_\eta$  at WG8 are smaller during the progression of the LB and LW tests. Both values are related to the erosion at WG8 which was smaller for the low dune tests than for the high dune tests. Figure 3.2 does not include the wet probability because the shoreline was located further landward of  $x = 18.6$  m where WG8 was installed. Therefore, the wet probability was  $P_w = 1$  for all wave gauges throughout the entire duration of the LB and LW tests.

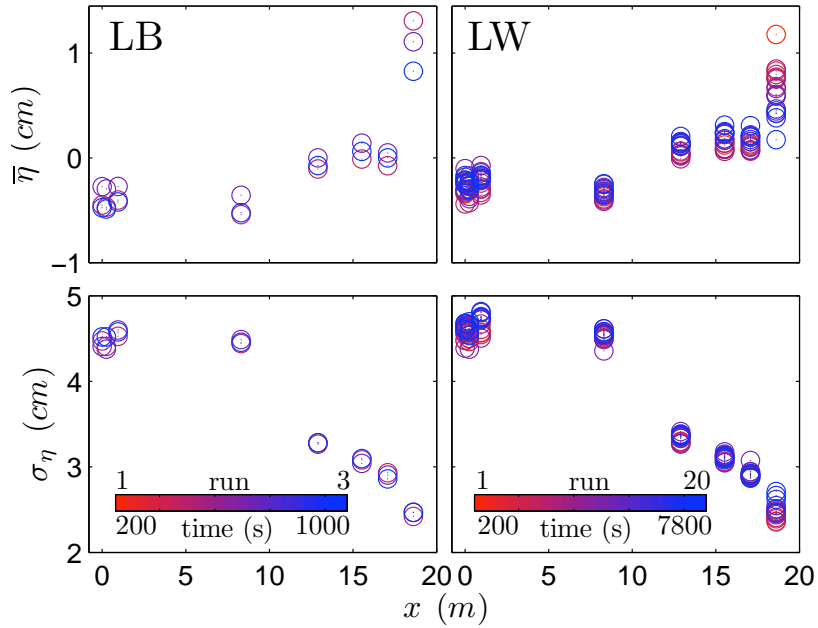


**Figure 3.2:** Cross-shore variations of mean (top) and standard deviation (bottom) of free surface elevation  $\eta$  for LB (left), and LW (right) tests.

**Table 3.6:** Mean free-surface elevation  $\bar{\eta}$  (cm) at eight wave gauge locations for the 6 runs of the HB test.

Run	WG1	WG2	WG3	WG4	WG5	WG6	WG7	WG8
HB1	-0.33	-0.37	-0.18	-0.28	0.11	0.31	0.20	4.17
HB2	-0.25	-0.28	-0.17	-0.26	0.17	0.31	0.20	4.88
HB3	-0.26	-0.26	-0.13	-0.27	0.10	0.31	0.22	4.55
HB4	-0.22	-0.20	-0.14	-0.23	0.12	0.25	0.14	4.50
HB5	-0.28	-0.30	-0.23	-0.31	0.02	0.22	0.14	3.91
HB6	-0.23	-0.27	0.18	-0.25	NR	0.27	0.16	1.57
Average	-0.26	-0.28	-0.17	-0.27	0.10	0.28	0.18	3.93

*NR implies "not reliable" data*

**Table 3.7:** Mean free-surface elevation  $\bar{\eta}$  (*cm*) at eight wave gauge locations for the 6 runs of the HN test.

<b>Run</b>	<b>WG1</b>	<b>WG2</b>	<b>WG3</b>	<b>WG4</b>	<b>WG5</b>	<b>WG6</b>	<b>WG7</b>	<b>WG8</b>
<b>HN1</b>	-0.12	-0.17	-0.04	-0.18	0.11	0.31	0.28	3.95
<b>HN2</b>	-0.15	-0.17	-0.13	-0.24	0.07	0.23	0.19	5.25
<b>HN3</b>	-0.18	-0.17	-0.10	-0.25	0.05	0.20	0.13	4.74
<b>HN4</b>	-0.20	-0.22	-0.20	-0.33	0.00	0.18	0.10	4.33
<b>HN5</b>	-0.23	-0.25	-0.20	-0.29	0.00	0.18	0.13	2.37
<b>HN6</b>	-0.25	-0.27	-0.20	-0.30	0.01	0.16	0.13	1.67
Average	-0.19	-0.21	-0.15	-0.27	0.04	0.21	0.16	3.67

**Table 3.8:** Mean free-surface elevation  $\bar{\eta}$  (*cm*) at eight wave gauge locations for the 28 runs of the HW test.

Run	WG1	WG2	WG3	WG4	WG5	WG6	WG7	WG8
HW1	-0.18	-0.22	-0.11	-0.25	0.06	0.30	0.07	4.60
HW2	-0.18	-0.18	-0.15	-0.25	0.08	0.30	0.15	4.74
HW3	-0.16	-0.18	-0.10	-0.20	0.02	0.23	0.10	4.45
HW4	-0.14	-0.15	-0.15	-0.11	0.03	0.24	0.08	4.48
HW5	-0.15	-0.14	-0.13	-0.22	NR	0.31	0.14	3.87
HW6	-0.17	-0.10	-0.07	-0.19	0.08	0.25	0.11	3.77
HW7	-0.13	-0.15	-0.18	-0.19	NR	0.29	0.12	3.08
HW8	-0.19	-0.14	-0.15	-0.23	0.01	0.27	0.12	2.30
HW9	-0.11	-0.15	-0.08	-0.21	0.08	0.26	0.19	2.17
HW10	-0.11	-0.08	-0.11	-0.24	0.07	0.27	0.18	2.08
HW11	-0.15	-0.15	-0.15	-0.19	0.07	0.28	0.16	1.98
HW12	-0.12	-0.11	-0.10	-0.21	0.14	0.34	0.22	1.99
HW13	-0.09	-0.10	-0.11	-0.14	0.18	0.36	0.23	1.88
HW14	-0.07	-0.10	-0.11	-0.21	0.16	0.31	0.18	1.68
HW15	-0.12	-0.14	-0.08	-0.18	0.12	0.21	0.17	1.70
HW16	-0.08	-0.08	-0.09	-0.18	0.18	0.33	0.18	1.65
HW17	-0.10	-0.09	-0.11	-0.19	0.18	0.32	0.19	1.64
HW18	-0.12	-0.12	-0.11	-0.21	NR	0.25	0.19	1.53
HW19	-0.09	-0.09	-0.11	-0.20	NR	0.31	0.21	1.51
HW20	-0.08	-0.10	-0.10	-0.19	NR	0.32	0.23	1.37
HW21	-0.14	-0.10	-0.08	-0.21	NR	0.21	0.19	1.36
HW22	-0.12	-0.14	-0.08	-0.20	NR	0.33	0.22	1.35
HW23	-0.08	-0.09	-0.09	-0.20	NR	0.32	0.26	1.32
HW24	-0.12	-0.12	-0.08	-0.19	NR	0.20	0.17	1.22
HW25	-0.08	-0.13	-0.12	-0.23	NR	0.33	0.19	1.27
HW26	-0.12	-0.11	-0.09	-0.23	NR	0.32	0.22	1.25
HW27	-0.13	-0.17	-0.12	-0.24	0.11	0.23	0.17	1.14
HW28	-0.19	-0.20	-0.16	-0.24	NR	0.22	0.16	1.05
Average	-0.13	-0.13	-0.11	-0.20	0.09	0.28	0.17	2.23

*NR implies "not reliable" data*

**Table 3.9:** Mean free-surface elevation  $\bar{\eta}$  (*cm*) at eight wave gauge locations for the 3 runs of the LB test.

<b>Run</b>	<b>WG1</b>	<b>WG2</b>	<b>WG3</b>	<b>WG4</b>	<b>WG5</b>	<b>WG6</b>	<b>WG7</b>	<b>WG8</b>
<b>LB1</b>	-0.45	-0.47	-0.40	-0.54	-0.11	-0.01	-0.08	1.31
<b>LB2</b>	-0.27	-0.30	-0.37	-0.36	0.00	0.14	0.05	1.11
<b>LB3</b>	-0.48	-0.49	-0.42	-0.52	-0.07	0.06	0.00	0.83
Average	-0.40	-0.42	-0.37	-0.47	-0.06	0.06	-0.01	1.08

**Table 3.10:** Mean free-surface elevation  $\bar{\eta}$  (cm) at eight wave gauge locations for the 20 runs of the LW test.

Run	WG1	WG2	WG3	WG4	WG5	WG6	WG7	WG8
LW1	-0.34	-0.31	-0.30	-0.37	0.03	0.12	0.12	1.18
LW2	-0.34	-0.33	-0.28	-0.37	0.04	0.13	0.08	NR
LW3	NR	NR	NR	NR	NR	NR	NR	0.83
LW4	-0.22	-0.30	-0.24	-0.34	0.03	0.08	0.06	0.76
LW5	-0.31	-0.26	-0.21	-0.35	0.06	0.14	0.13	0.80
LW6	-0.33	-0.31	-0.33	-0.36	0.07	0.08	0.11	0.75
LW7	-0.44	-0.43	-0.35	-0.41	-0.01	0.06	0.08	0.68
LW8	-0.22	-0.27	-0.13	-0.32	0.14	0.14	0.16	0.77
LW9	-0.30	-0.37	-0.29	-0.39	0.04	0.09	0.07	0.59
LW10	NR	NR	NR	NR	NR	NR	NR	0.85
LW11	-0.32	-0.39	-0.28	-0.40	0.02	0.08	0.08	0.60
LW12	-0.10	-0.17	-0.07	-0.28	0.15	0.22	0.20	0.66
LW13	-0.31	-0.30	-0.20	-0.32	0.12	0.17	0.20	0.59
LW14	-0.24	-0.30	-0.18	-0.32	0.12	0.17	0.10	0.45
LW15	-0.21	-0.24	-0.21	-0.30	0.11	0.23	0.22	0.43
LW16	-0.23	-0.26	-0.17	-0.29	0.14	0.24	0.15	NR
LW17	-0.17	-0.22	-0.14	-0.25	0.16	0.18	0.18	0.42
LW18	-0.19	-0.27	-0.22	-0.36	0.11	0.24	0.21	0.47
LW19	-0.21	-0.23	-0.19	-0.25	0.21	0.31	0.31	0.38
LW20	-0.25	-0.30	-0.17	-0.34	0.14	0.25	0.20	0.17
Average	-0.26	-0.29	-0.22	-0.33	0.09	0.16	0.15	0.63

*NR implies "not reliable" data*

**Table 3.11:** Free-surface standard deviation  $\sigma_\eta$  (cm) at eight wave gauge locations for the 6 runs of the HB test.

Run	WG1	WG2	WG3	WG4	WG5	WG6	WG7	WG8
<b>HB1</b>	4.57	4.58	4.68	4.47	3.27	3.19	3.09	1.96
<b>HB2</b>	4.69	4.67	4.75	4.57	3.35	3.26	3.22	1.99
<b>HB3</b>	4.66	4.61	4.71	4.54	3.31	3.22	3.21	1.96
<b>HB4</b>	4.66	4.67	4.71	4.53	3.29	3.25	3.20	2.03
<b>HB5</b>	4.66	4.63	4.72	4.55	3.27	3.23	3.19	2.03
<b>HB6</b>	4.60	4.60	4.72	4.45	NR	3.15	3.05	2.48
Average	4.64	4.63	4.72	4.52	3.30	3.22	3.16	2.08

*NR implies "not reliable" data*

**Table 3.12:** Free-surface standard deviation  $\sigma_\eta$  (*cm*) at eight wave gauge locations for the 6 runs of the HN test.

<b>Run</b>	<b>WG1</b>	<b>WG2</b>	<b>WG3</b>	<b>WG4</b>	<b>WG5</b>	<b>WG6</b>	<b>WG7</b>	<b>WG8</b>
<b>HN1</b>	4.59	4.52	4.72	4.62	3.47	3.36	3.24	1.87
<b>HN2</b>	4.67	4.65	4.72	4.63	3.46	3.36	3.27	1.92
<b>HN3</b>	4.63	4.58	4.72	4.61	3.45	3.38	3.26	1.96
<b>HN4</b>	4.74	4.67	4.74	4.65	3.50	3.38	3.30	2.03
<b>HN5</b>	4.72	4.70	4.73	4.62	3.44	3.30	3.17	2.25
<b>HN6</b>	4.57	4.54	4.64	4.50	3.43	3.24	3.09	2.46
Average	4.65	4.61	4.71	4.60	3.46	3.34	3.22	2.08

**Table 3.13:** Free-surface standard deviation  $\sigma_\eta$  ( $cm$ ) at eight wave gauge locations for the 28 runs of the HW test.

	<b>WG1</b>	<b>WG2</b>	<b>WG3</b>	<b>WG4</b>	<b>WG5</b>	<b>WG6</b>	<b>WG7</b>	<b>WG8</b>
<b>HW1</b>	4.53	4.54	4.65	4.57	3.38	3.33	3.20	1.89
<b>HW2</b>	4.57	4.60	4.70	4.60	3.40	3.36	3.24	2.00
<b>HW3</b>	4.65	4.62	4.70	4.63	3.38	3.38	3.29	2.03
<b>HW4</b>	4.60	4.57	4.69	4.59	3.35	3.32	3.26	2.02
<b>HW5</b>	4.62	4.60	4.68	4.55	NR	3.29	3.27	2.04
<b>HW6</b>	4.60	4.58	4.68	4.57	3.28	3.28	3.26	2.07
<b>HW7</b>	4.62	4.60	4.70	4.59	3.12	3.28	3.23	2.10
<b>HW8</b>	4.64	4.59	4.71	4.59	3.31	3.28	3.22	2.24
<b>HW9</b>	4.65	4.61	4.70	4.59	3.39	3.29	3.25	2.28
<b>HW10</b>	4.65	4.62	4.67	4.61	3.39	3.29	3.21	2.27
<b>HW11</b>	4.69	4.66	4.68	4.61	3.37	3.30	3.18	2.30
<b>HW12</b>	4.70	4.68	4.70	4.61	3.39	3.29	3.17	2.32
<b>HW13</b>	4.72	4.69	4.72	4.61	3.40	3.28	3.17	2.31
<b>HW14</b>	4.73	4.71	4.70	4.60	3.38	3.31	3.16	2.33
<b>HW15</b>	4.60	4.58	4.69	4.56	3.39	3.27	3.12	2.36
<b>HW16</b>	4.65	4.63	4.73	4.59	3.42	3.27	3.13	2.40
<b>HW17</b>	4.65	4.63	4.72	4.58	3.43	3.27	3.11	2.41
<b>HW18</b>	4.57	4.53	4.63	4.52	NR	3.24	3.08	2.39
<b>HW19</b>	4.61	4.57	4.67	4.53	NR	3.23	3.08	2.40
<b>HW20</b>	4.62	4.59	4.68	4.56	NR	3.25	3.07	2.38
<b>HW21</b>	4.59	4.57	4.66	4.56	NR	3.22	3.05	2.43
<b>HW22</b>	4.61	4.58	4.68	4.56	NR	3.23	3.04	2.46
<b>HW23</b>	4.60	4.57	4.66	4.56	NR	3.23	3.04	2.44
<b>HW24</b>	4.50	4.46	4.57	4.48	NR	3.18	3.02	2.40
<b>HW25</b>	4.53	4.50	4.60	4.50	NR	3.20	2.99	2.43
<b>HW26</b>	4.57	4.54	4.62	4.54	NR	3.21	2.99	2.43
<b>HW27</b>	4.53	4.50	4.59	4.55	3.43	3.20	2.98	2.46
<b>HW28</b>	4.52	4.49	4.55	4.50	NR	3.15	2.93	2.40
<b>Average</b>	4.61	4.59	4.67	4.57	3.37	3.27	3.13	2.28

*NR implies "not reliable" data*

**Table 3.14:** Free-surface standard deviation  $\sigma_\eta$  (*cm*) at eight wave gauge locations for the 3 runs of the LB test.

	<b>WG1</b>	<b>WG2</b>	<b>WG3</b>	<b>WG4</b>	<b>WG5</b>	<b>WG6</b>	<b>WG7</b>	<b>WG8</b>
<b>LB1</b>	4.47	4.41	4.53	4.44	3.26	3.08	2.93	2.42
<b>LB2</b>	4.41	4.38	4.60	4.49	3.28	3.04	2.90	2.47
<b>LB3</b>	4.52	4.52	4.58	4.46	3.28	3.10	2.86	2.47
<b>Average</b>	4.47	4.43	4.57	4.46	3.28	3.07	2.90	2.45

**Table 3.15:** Free-surface standard deviation  $\sigma_\eta$  (cm) at eight wave gauge locations for the 20 runs of the LW test.

	<b>WG1</b>	<b>WG2</b>	<b>WG3</b>	<b>WG4</b>	<b>WG5</b>	<b>WG6</b>	<b>WG7</b>	<b>WG8</b>
<b>LW1</b>	4.48	4.50	4.57	4.51	3.30	3.12	2.94	2.49
<b>LW2</b>	NR							
<b>LW3</b>	NR	2.36						
<b>LW4</b>	4.58	4.57	4.57	4.55	3.35	3.11	2.91	2.36
<b>LW5</b>	4.48	4.46	4.55	4.49	3.28	3.06	2.90	2.39
<b>LW6</b>	4.57	4.55	4.61	4.54	3.28	3.05	2.88	2.41
<b>LW7</b>	4.55	4.50	4.67	4.52	3.29	3.06	2.87	2.51
<b>LW8</b>	4.65	4.61	4.72	4.58	3.36	3.13	2.91	2.46
<b>LW9</b>	4.65	4.64	4.75	4.57	3.36	3.12	2.89	2.46
<b>LW10</b>	NR	2.46						
<b>LW11</b>	4.64	4.61	4.73	4.56	3.37	3.14	2.91	2.44
<b>LW12</b>	4.39	4.38	4.51	4.36	3.27	3.05	3.07	2.47
<b>LW13</b>	4.68	4.65	4.76	4.61	3.41	3.17	2.94	2.45
<b>LW14</b>	4.62	4.60	4.72	4.53	3.34	3.10	2.90	2.48
<b>LW15</b>	4.59	4.59	4.72	4.50	3.33	3.09	2.87	2.51
<b>LW16</b>	4.61	4.58	4.74	4.55	3.37	3.15	2.92	NR
<b>LW17</b>	4.62	4.59	4.74	4.55	3.36	3.13	2.88	2.62
<b>LW18</b>	4.67	4.66	4.80	4.58	3.38	3.12	2.90	2.55
<b>LW19</b>	4.68	4.70	4.82	4.61	3.38	3.11	2.92	2.66
<b>LW20</b>	4.61	4.54	4.75	4.55	3.36	3.08	2.87	2.71
<b>Average</b>	4.61	4.59	4.71	4.56	3.36	3.13	2.93	2.49

*NR implies "not reliable" data*

**Table 3.16:** Wet probability  $P_w$  for WG8 for the high dune test series.

<b>Run</b>	<b>HB</b>	<b>HN</b>	<b>HW</b>
<b>1</b>	0.91	0.89	0.89
<b>2</b>	0.87	0.84	0.87
<b>3</b>	0.85	0.85	0.88
<b>4</b>	0.86	0.86	0.89
<b>5</b>	0.86	0.90	0.90
<b>6</b>	1	1	0.90
<b>7</b>			0.90
<b>8-28</b>			1
<b>Average</b>	0.89	0.89	0.89

### 3.1.3 Velocity

Fluid velocity was recorded by one 2D ADV sensor co-located with WG5 ( $x = 12.9\text{ m}$ ) and two Vectrinos co-located with WG6 at  $x = 15.5\text{ m}$  (blue Vectrino) and WG7 at  $x = 17.1\text{ m}$  (red Vectrino). All three velocimeters have sideways looking probe tips suitable for measurements in shallower water. The sampling volume of all velocimeters was placed at  $2/3$  of the local water depth  $d$  below  $SWL$  above the local bottom at the beginning of each run. Besides guaranteeing for measurements well outside the bottom boundary layer with enough clearance to prevent scouring caused by the probe tip, this elevation minimized the negative effects of entrained air bubbles on the velocity measurement. Furthermore, the chosen measurement location is assumed to give a fairly good representation of the depth-averaged velocities. While the 2D ADV is limited to measure cross-shore ( $u$ ) and alongshore ( $v$ ) velocities, the Vectrinos also measure the vertical ( $w$ ) velocity. The cross-shore velocity component  $u$  was measured to be dominant as expected in this two-dimensional wave flume experiment. Measured alongshore and vertical velocities were small in comparison to the cross-shore velocities. The statistical values of all the velocity data are presented in Appendix (Table A.6 to A.20).

The mean cross-shore velocity ( $\bar{u}$ ) and its respective standard deviation ( $\sigma_u$ ) for all velocimeters are listed in Table 3.17 to 3.21. The calculated average values of  $\bar{u}$  and  $\sigma_u$  are listed at the bottom of each table. Additionally, the cross-shore and temporal variations of the tabulated velocity statistics are illustrated in Figure 3.3 for the high dune tests and in Figure 3.4 for the low dune tests. As explained in the previous chapter, the temporal variation is represented by the color scheme ranging from red (first wave run) to blue (last wave run). Since each value represents an average over the specific  $400 - s$  wave run, the data points are plotted in the middle of each respective run.

The value of  $\bar{u}$  (negative for offshore undertow current) and its respective standard deviation  $\sigma_u$  in Figure 3.3 show only minor variations in the inner surf zone ( $x = 12.9 - 17.1\text{ m}$ ) during each test. The calculated average values of  $\bar{u}$  range from

$-4.97$  to  $-5.24$   $cm/s$  for the 2D ADV. The ranges are between  $-3.28$  to  $-4.33$   $cm/s$ , and  $-4.08$  to  $-5.15$   $cm/s$  for the blue and red Vectrinos, respectively. The mean cross-shore velocity is negative and due to an undertow current. The current decreases from  $x = 12.9$   $m$  to  $x = 15.5$   $m$  before it increases at  $x = 17.1$   $m$  where some broken waves in the inner surf zone broke again on the steeper bottom slope. Between  $x = 12.9 - 15.5$   $m$   $\sigma_u$  varied little and increased at  $x = 17.1$   $m$  probably due to the increased wave breaking on the steeper bottom slope. The velocity data for the low dune test series are shown in Figure 3.4 and are similar to those of the high dune tests.

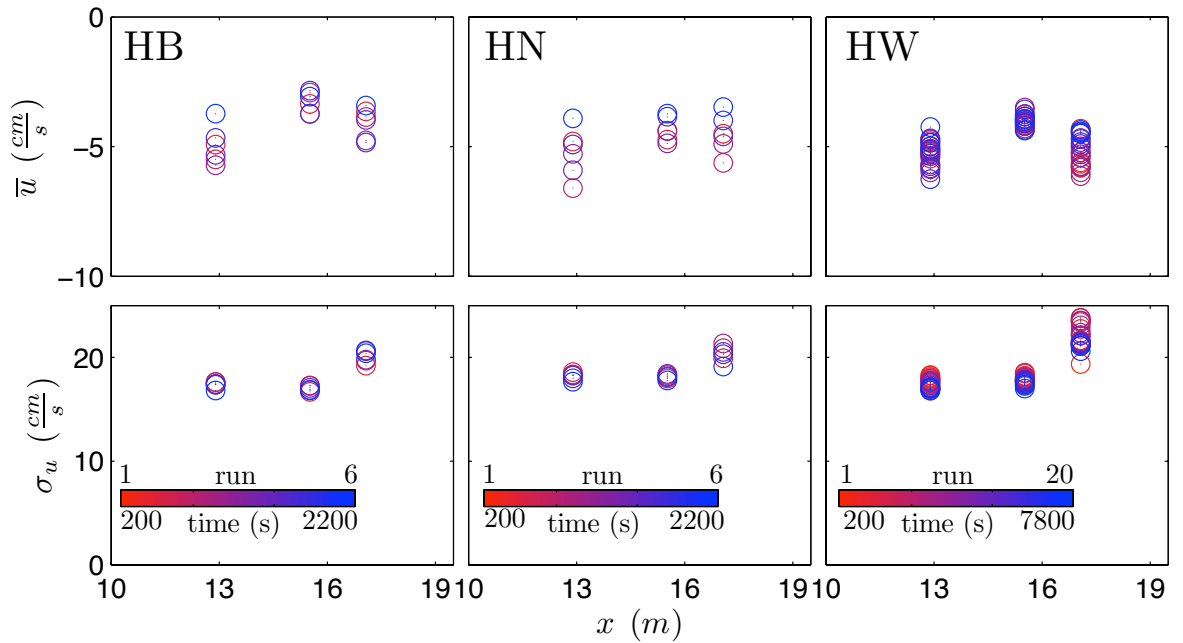


**Figure 3.3:** Temporal variations of the mean (top) and standard deviation (bottom) of the cross-shore velocity at the three velocimeters during the HB (left), HN (middle), and HW (right) tests.

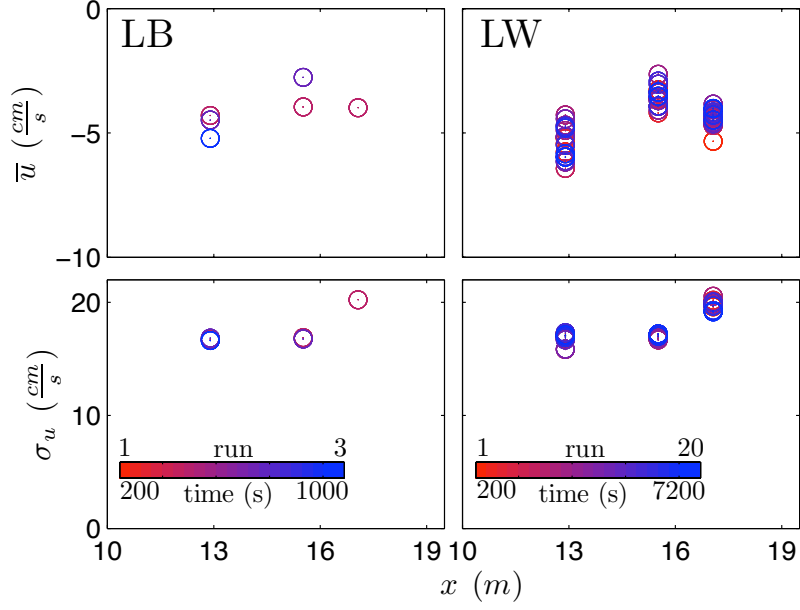


**Figure 3.4:** Temporal variations of the mean (top) and standard deviation (bottom) of the cross-shore velocity at the three velocimeters during the LB (left), and LW (right) tests.

**Table 3.17:** Mean cross-shore  $\bar{u}$  and its standard deviation  $\sigma_u$  of the 2D ADV co-located with WG5 at  $x = 12.90\text{ m}$ , blue Vectrino co-located with WG6 at  $x = 15.52\text{ m}$  and red Vectrino co-located with WG7 at  $x = 17.07\text{ m}$  for the HB Test.

Run	2D ADV at WG5		blue Vectrino at WG6		red Vectrino at WG7	
	$\bar{u}$ (cm/s)	$\sigma_u$ (cm/s)	$\bar{u}$ (cm/s)	$\sigma_u$ (cm/s)	$\bar{u}$ (cm/s)	$\sigma_u$ (cm/s)
<b>HB1</b>	-4.92	17.61	-3.35	16.68	-3.64	19.20
<b>HB2</b>	-5.49	17.64	-2.92	17.29	-2.86	19.69
<b>HB3</b>	-5.72	17.40	-3.73	17.27	-4.76	19.78
<b>HB4</b>	-5.31	17.45	-3.74	17.07	-3.97	20.60
<b>HB5</b>	-4.66	17.38	-2.84	16.84	-4.84	20.67
<b>HB6</b>	-3.73	16.81	-3.07	16.89	-3.42	20.39
Average	-4.97	17.38	-3.28	17.01	-4.08	20.06

**Table 3.18:** Mean cross-shore  $\bar{u}$  and its standard deviation  $\sigma_u$  of the 2D ADV co-located with WG5 at  $x = 12.90 m$ , blue Vectrino co-located with WG6 at  $x = 15.52 m$  and red Vectrino co-located with WG7 at  $x = 17.07 m$  for the HN test.

Run	2D ADV at WG5		blue Vectrino at WG6		red Vectrino at WG7	
	$\bar{u}$ (cm/s)	$\sigma_u$ (cm/s)	$\bar{u}$ (cm/s)	$\sigma_u$ (cm/s)	$\bar{u}$ (cm/s)	$\sigma_u$ (cm/s)
<b>HN1</b>	-4.80	18.58	-4.73	17.97	-4.50	19.91
<b>HN2</b>	-6.60	18.27	-4.39	18.17	-4.63	20.88
<b>HN3</b>	-5.28	18.36	-4.40	18.42	-4.89	21.34
<b>HN4</b>	-5.91	18.26	-4.87	18.31	-4.60	20.53
<b>HN5</b>	-4.92	18.00	-3.85	18.10	-3.99	20.31
<b>HN6</b>	-3.91	17.65	-3.73	17.78	-3.47	19.13
Average	-5.24	18.19	-4.33	18.13	-4.51	20.35

**Table 3.19:** Mean cross-shore  $\bar{u}$  and its standard deviation  $\sigma_u$  of the 2D ADV co-located with WG5 at  $x = 12.90 m$ , blue Vectrino co-located with WG6 at  $x = 15.52 m$  and red Vectrino co-located with WG7 at  $x = 17.07 m$  for the HW test.

Run	2D ADV at WG5		blue Vectrino at WG6		red Vectrino at WG7	
	$\bar{u}$ (cm/s)	$\sigma_u$ (cm/s)	$\bar{u}$ (cm/s)	$\sigma_u$ (cm/s)	$\bar{u}$ (cm/s)	$\sigma_u$ (cm/s)
HW1	-4.71	18.11	NR	NR	-4.32	19.36
HW2	-5.10	18.24	-4.19	18.03	-5.67	21.67
HW3	-5.46	18.29	NR	NR	-5.60	22.76
HW4	-4.79	17.98	-4.10	18.53	-5.81	21.35
HW5	-5.17	18.01	-4.22	18.43	-5.41	23.56
HW6	-5.37	17.94	-3.96	18.24	-5.75	23.78
HW7	NR	NR	NR	NR	NR	NR
HW8	-4.98	17.79	-4.09	18.16	-5.80	23.40
HW9	-5.24	17.69	-3.76	18.04	-5.22	23.09
HW10	-5.14	17.81	-3.93	18.05	-5.98	23.83
HW11	-5.69	17.11	NR	NR	-6.13	23.52
HW12	-5.20	17.59	-3.49	17.92	-5.22	23.54
HW13	-6.00	17.53	-4.16	17.78	-5.04	22.38
HW14	-5.68	17.32	-4.30	17.67	-4.99	22.09
HW15	-4.68	17.43	-4.22	17.74	-5.30	22.13
HW16	-5.84	17.63	-3.74	17.77	-5.41	21.44
HW17	-5.36	17.32	-4.03	17.58	-5.75	21.51
HW18	-4.85	17.09	-4.02	17.65	-4.67	21.57
HW19	-5.87	16.84	-3.94	17.79	-4.83	21.32
HW20	-5.12	17.00	-4.11	17.88	NR	NR
HW21	-4.72	16.80	-3.84	17.80	-4.71	21.27
HW22	-5.08	17.00	-4.01	17.72	-4.41	21.34
HW23	-5.75	17.10	-4.08	17.56	-4.90	21.37
HW24	-5.28	17.17	-3.56	17.39	-4.47	21.13
HW25	-5.00	16.83	-4.35	17.51	-4.36	21.14
HW26	-6.26	17.00	-3.94	17.26	NR	NR
HW27	-4.24	17.01	-4.38	17.36	-4.50	21.10
HW28	-4.84	16.98	-3.84	17.01	-4.44	20.60
Average	-5.24	17.45	-4.01	17.79	-5.15	22.01

*NR implies "not reliable" data*

**Table 3.20:** Mean cross-shore  $\bar{u}$  and its standard deviation  $\sigma_u$  of the 2D ADV co-located with WG5 at  $x = 12.90\text{ m}$ , blue Vectrino co-located with WG6 at  $x = 15.52\text{ m}$  and red Vectrino co-located with WG7 at  $x = 17.07\text{ m}$  for the LB test.

Run	2D ADV at WG5		blue Vectrino at WG6		red Vectrino at WG7	
	$\bar{u}$ (cm/s)	$\sigma_u$ (cm/s)	$\bar{u}$ (cm/s)	$\sigma_u$ (cm/s)	$\bar{u}$ (cm/s)	$\sigma_u$ (cm/s)
<b>LB1</b>	-4.31	16.68	-3.96	16.89	-3.99	20.23
<b>LB2</b>	-4.48	16.83	-2.77	16.77	NR	NR
<b>LB3</b>	-5.21	16.62	NR	NR	NR	NR
Average	-4.67	16.71	-3.37	16.83	-3.99	20.23

*NR implies "not reliable" data*

**Table 3.21:** Mean cross-shore  $\bar{u}$  and its standard deviation  $\sigma_u$  of the 2D ADV co-located with WG5 at  $x = 12.90\text{ m}$ , blue Vectrino co-located with WG6 at  $x = 15.52\text{ m}$  and red Vectrino co-located with WG7 at  $x = 17.07\text{ m}$  for the LW test.

Run	2D ADV at WG5		blue Vectrino at WG6		red Vectrino at WG7	
	$\bar{u}$ (cm/s)	$\sigma_u$ (cm/s)	$\bar{u}$ (cm/s)	$\sigma_u$ (cm/s)	$\bar{u}$ (cm/s)	$\sigma_u$ (cm/s)
LW1	-5.42	17.04	-3.91	17.15	-5.34	19.61
LW2	-5.76	17.30	-3.27	17.14	-4.47	20.07
LW3	-5.22	17.10	-4.20	16.81	-4.65	20.18
LW4	-5.15	16.99	NR	NR	-4.64	20.10
LW5	-5.18	17.08	-3.60	16.95	-4.40	20.00
LW6	-6.42	17.26	-3.65	16.69	-4.70	19.96
LW7	-5.97	16.74	-3.35	17.06	-4.42	19.98
LW8	-4.28	15.83	-3.39	16.98	-4.49	20.52
LW9	-4.90	17.06	-2.64	16.86	-4.07	19.85
LW10	-4.69	17.02	-4.08	16.71	-4.35	20.07
LW11	-6.17	16.88	-3.56	16.83	-3.84	19.72
LW12	-4.43	15.88	-3.70	17.15	NR	NR
LW13	-5.13	16.69	-3.94	17.19	-4.58	19.75
LW14	-6.12	17.05	NR	NR	-4.63	20.01
LW15	-5.95	17.06	-3.05	17.17	-4.22	20.03
LW16	-5.49	17.32	-2.91	17.21	-4.16	20.02
LW17	-4.73	17.01	-3.92	17.20	-4.03	19.68
LW18	-4.80	16.88	NR	NR	-4.29	19.28
LW19	-5.84	17.15	-3.52	17.00	-4.49	19.20
LW20	-5.98	17.09	-3.36	17.20	-4.01	19.17
Average	-5.38	16.92	-3.53	17.02	-4.41	19.85

*NR implies "not reliable" data*

## 3.2 Morphology and Overwash

The main focus of this study is the measurement of profile evolution of bare and vegetated dunes in presence of wave overtopping and overwash. The evaluation of the measured morphological changes and overwash quantities is important to gain a better understanding of vegetation effects on dune and beach profile evolution. Measured bottom elevations are averaged alongshore to obtain  $2D$  beach and dune profiles as a function of  $x$  at time  $t$ . Scarping and slumping processes were observed on the foredune of the high dune test series but not for the low dune test series. For every run the water and sediment volumes carried over the vertical wall crest at the landward end of the dune were measured after each  $400 - s$  run. To collect the overwashed sediment volume, the overtopped water containing sand particles was forced through a horizontal streamer trap with a fine polyester fabric mesh. The collected overtopped water and overwashed sand volumes as explained in Chapter 2.1 are converted to the transport rates in the following chapter.

### 3.2.1 Transport Rates

For clarity, the explanations in Chapter 2.1 are elaborated further. The wet sand was removed from the trap after each run and its wet mass ( $W_{ws}$ ) was determined. After drying the wet sand in an oven for  $24$  hours it was weighted again to obtain the weight of the dry sand ( $W_{ds}$ ). The difference between these two values ( $W_{ws} - W_{ds}$ ), was the water mass in the wet sand. In cases of major overwash only a sample of the wet sand was dried and weighted to obtain the ratios of the water and sand in the wet sand. This water mass was converted to the water volume retained in the wet sand. Furthermore, the water volume collected in the collection basin and the volume pumped back into the wave flume during the run were added to obtain the total water volume transported over the vertical wall. Measurement errors of the pumped volume were determined to be below 2% by Figlus et al. (2009). The volume per unit width of the overwash sand (bedload and suspended load) excluding voids ( $V_{bs}$ ) was calculated by dividing the entire dry sand mass ( $cm^3$ ) by the density of quartz sand  $\rho = 2.6 g/cm^3$  and the

width of the flume (115 m). The water volume per unit width,  $V_{mo}$ , was obtained by dividing the total water volume ( $cm^3$ ) by the flume width of 115 m. The average sand overwash rate ( $q_{bs}$ ) and water overtopping rate ( $q_o$ ) were calculated by dividing  $V_{bs}$  and  $V_{mo}$  by the run duration of 400 s.

The temporal variations of the measured transport rates and their ratio are shown in Figures 3.5 and 3.6 for the high and low dune test series, respectively. The measured beach and dune profile evolutions are presented in Chapter 3.2.2 although the profile evolutions are discussed to interpret these figures. The water overtopping rate  $q_o$  (top panel), the sediment overwash rate  $q_{bs}$  (middle panel), and the ratio of those two values (bottom panel) are shown in these figures. The transport rates ( $cm^2/s$ ) represent averages over the respective run lasting 400 s. Therefore, each data point is plotted at time  $t$  corresponding to the middle of each run. The corresponding values are listed in Table 3.22 to 3.26.

The wave overtopping rate for the HB (red, circles) and HN (green, squares) tests increased rapidly with time after the third run ( $t = 1,200$  s). For the HW test (blue, diamonds), however, wave overtopping did not occur until the end of run 20 (8,000 s). Therefore,  $q_{bs}$  and  $q_o$  were zero for the duration from HW1 to HW20 where the integer affixed to the test name indicates the run number starting from run number 0 for the initial profile. When backdune erosion started and slowly progressed the value of  $q_o$  increased but remained relatively small until the end of the test which was terminated due to alongshore variability. The HB and HN tests were stopped when  $q_o$  and  $q_{bs}$  reached the upper limit of about  $18\text{ cm}^2/s$  and  $0.5\text{ cm}^2/s$ , respectively, in the previous experiment with no vegetation conducted by Figlus et al. (2009). The upper limit occurred when the dune crest was at the same elevation as the vertical wall crest. The overtopping (overwash) rate of the last run of the HB, HN, and HW tests was  $q_o = 18.89\text{ cm}^2/s$  ( $q_{bs} = 0.52\text{ cm}^2/s$ ),  $q_o = 17.25\text{ cm}^2/s$  ( $q_{bs} = 0.39\text{ cm}^2/s$ ), and  $q_o = 2.67\text{ cm}^2/s$  ( $q_{bs} = 0.10\text{ cm}^2/s$ ), respectively. At the beginning of wave overtopping and overwash, the ratio, which represents the volumetric sand concentration in the overtopping flow, was about 0.2 in all three tests. This may have been caused by

transport of loose sand particles on the surface. The ratio decreased with the increase of the wave overtopping rate. The ratio for the HW test decreased at a slower rate which suggests that vegetation may have generated additional turbulence and increased sand concentration. The similarity of the overtopping and overwash rates for the HB and HN tests clearly shows that the narrow vegetation on the steep backdune did not reduce backdune erosion caused by the overtopping flow. On the other hand, the wide vegetation covering the entire dune was effective in reducing  $q_o$  and  $q_{bs}$  because it protected the dune against direct wave attack and reduced dune scarping as will be shown in the next Chapter [3.2.2](#).

Figure [3.6](#) shows the temporal variations of  $q_o$ ,  $q_{bs}$  and  $q_{bs}/q_o$  for the low dune test series. The wide vegetation reduced the wave overtopping rate and the sand overwash rate by a factor of above 3 and 2, respectively. The wide vegetation retarded wave uprush on the upward slope in the swash and inner surf zone. The overtopping rate remained almost constant throughout the LW test. Furthermore, the sand overwash rate decreased with the progression of erosion in front of the vertical possibly because of the reduced availability of sand in the overtopping flow. The wide vegetation was effective in reducing  $q_o$  even after its seaward segment was situated in the inner surf zone (see Chapter [3.2.2](#)). In reality, woody plants could be destroyed by the wave force or uprooted due to erosion. These factors were not considered in this experiment. The ratio  $q_o/q_{bs}$  was larger for the wide vegetation which may have been caused by the increased turbulence and suspended sand concentration in the vegetated zone.

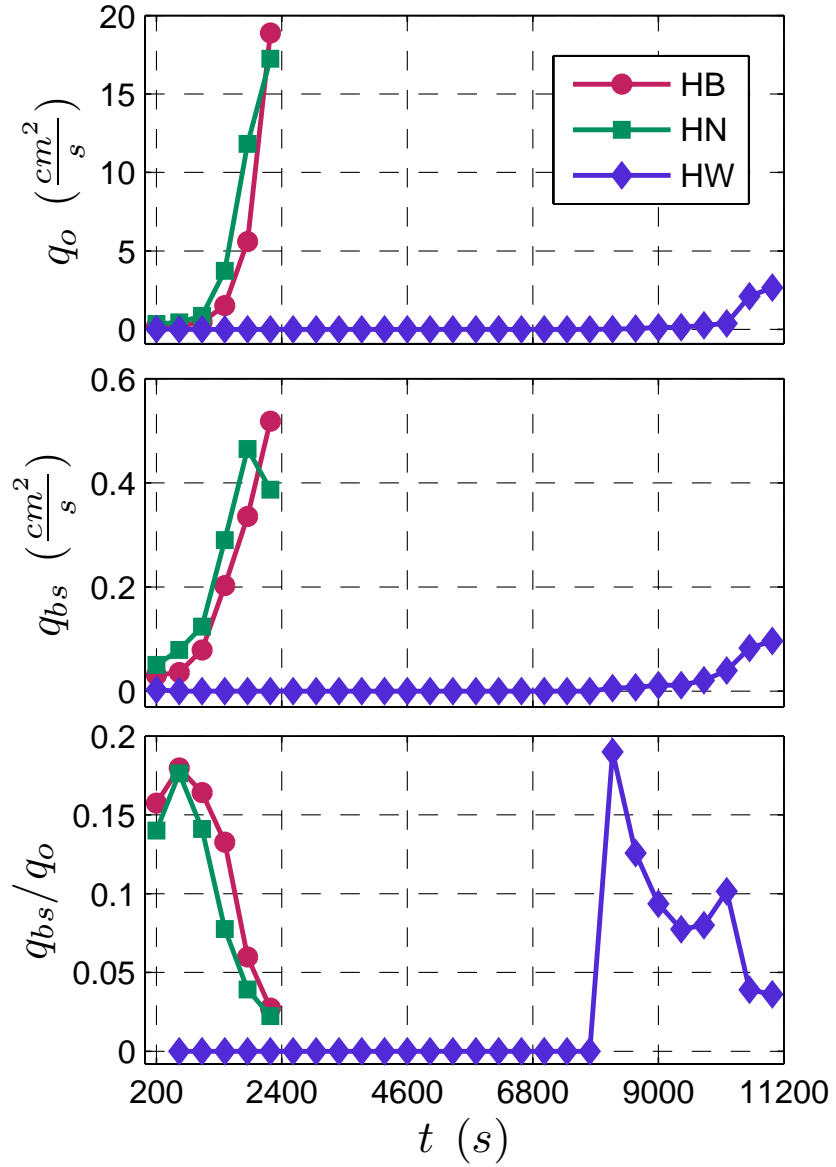


**Figure 3.5:** Temporal variations of wave overtopping rate  $q_o$  (top), sand overwash rate  $q_{bs}$  (middle), and ratio  $q_{bs}/q_o$  (bottom) for the high dune test series.

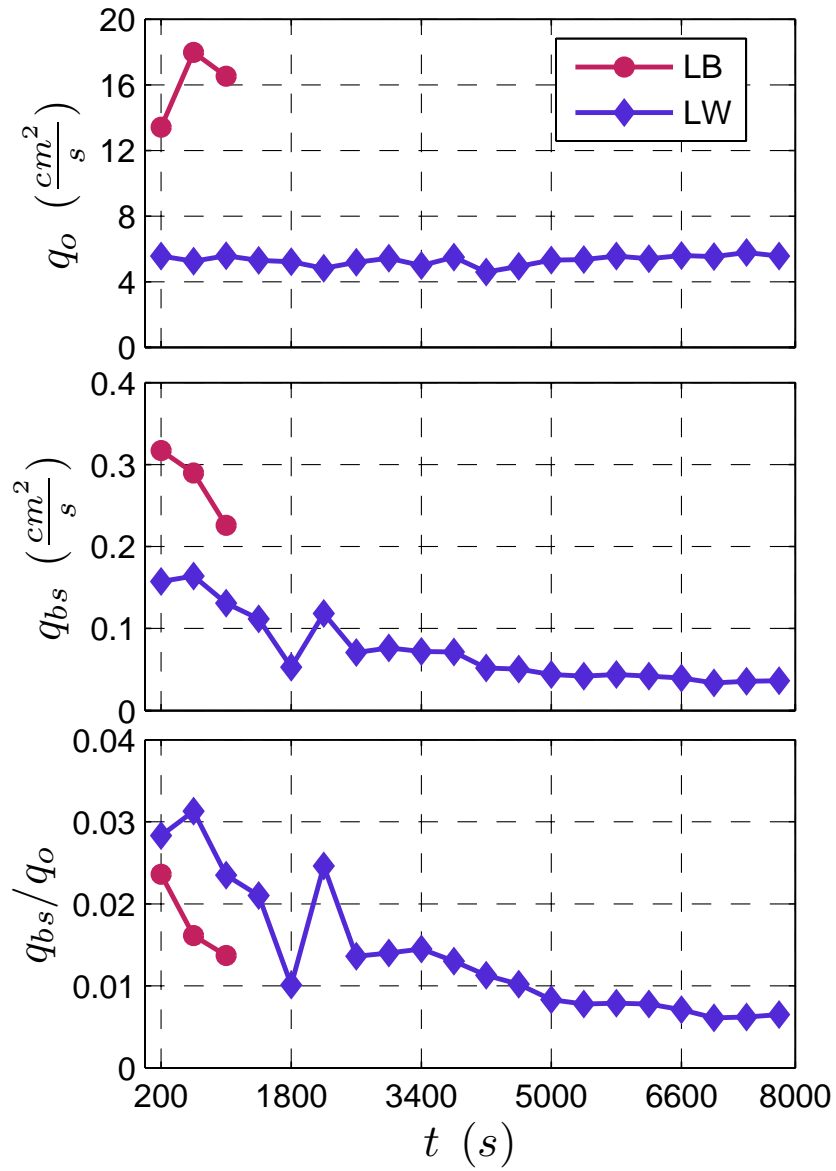


**Figure 3.6:** Temporal variations of wave overtopping rate  $q_o$  (top), sand overwash rate  $q_{bs}$  (middle), and ratio  $q_{bs}/q_o$  (bottom) for the low dune test series.

**Table 3.22:** Measured sediment overwash rate ( $q_{bs}$ ), water overtopping rate ( $q_o$ ), and their ratio for the 6 runs of the HB test.

<b>Run</b>	$q_{bs}$ ( $cm^2/s$ )	$q_o$ ( $cm^2/s$ )	$q_{bs}/q_o$
<b>HB1</b>	0.03	0.19	0.16
<b>HB2</b>	0.04	0.20	0.18
<b>HB3</b>	0.07	0.48	0.16
<b>HB4</b>	0.20	1.53	0.13
<b>HB5</b>	0.34	5.60	0.06
<b>HB6</b>	0.52	18.89	0.03

**Table 3.23:** Measured sediment overwash rate ( $q_{bs}$ ), water overtopping rate ( $q_o$ ), and their ratio for the 6 runs of the HN test.

<b>Run</b>	$q_{bs}$ ( $cm^2/s$ )	$q_o$ ( $cm^2/s$ )	$q_{bs}/q_o$
<b>HN1</b>	0.05	0.36	0.14
<b>HN2</b>	0.08	0.45	0.18
<b>HN3</b>	0.12	0.88	0.14
<b>HN4</b>	0.29	3.73	0.08
<b>HN5</b>	0.46	11.81	0.04
<b>HN6</b>	0.39	17.25	0.02

**Table 3.24:** Measured sediment overwash rate ( $q_{bs}$ ), water overtopping rate ( $q_o$ ), and their ratio for the 28 runs of the HW test.

<b>Run</b>	$q_{bs}$ ( $cm^2/s$ )	$q_o$ ( $cm^2/s$ )	$q_{bs}/q_o$
<b>HW1</b>	0.003	0.0191	0.15
<b>HW21</b>	0.0059	0.0311	0.19
<b>HW22</b>	0.0074	0.0585	0.13
<b>HW23</b>	0.0113	0.1204	0.09
<b>HW24</b>	0.0114	0.1477	0.08
<b>HW25</b>	0.0210	0.2628	0.08
<b>HW26</b>	0.0395	0.3887	0.10
<b>HW27</b>	0.0827	2.1202	0.04
<b>HW28</b>	0.0965	2.6743	0.04

**Table 3.25:** Measured sediment overwash rate ( $q_{bs}$ ), water overtopping rate ( $q_o$ ), and their ratio for the 3 runs of the LB test.

<b>Run</b>	$q_{bs}$ ( $cm^2/s$ )	$q_o$ ( $cm^2/s$ )	$q_{bs}/q_o$
<b>LB1</b>	0.32	13.42	0.02
<b>LB2</b>	0.29	17.98	0.02
<b>LB3</b>	0.23	16.52	0.01

**Table 3.26:** Measured sediment overwash rate ( $q_{bs}$ ), water overtopping rate ( $q_o$ ), and their ratio for the 20 runs of the LW test.

<b>Run</b>	$q_{bs}$ ( $cm^2/s$ )	$q_o$ ( $cm^2/s$ )	$q_{bs}/q_o$
<b>LW1</b>	0.16	5.57	0.03
<b>LW2</b>	0.16	5.24	0.03
<b>LW3</b>	0.13	5.58	0.02
<b>LW4</b>	0.11	5.30	0.02
<b>LW5</b>	0.05	5.21	0.01
<b>LW6</b>	0.12	4.81	0.02
<b>LW7</b>	0.07	5.19	0.01
<b>LW8</b>	0.08	5.43	0.01
<b>LW9</b>	0.07	4.99	0.01
<b>LW10</b>	0.07	5.50	0.01
<b>LW11</b>	0.05	4.59	0.01
<b>LW12</b>	0.05	4.93	0.01
<b>LW13</b>	0.04	5.32	0.01
<b>LW14</b>	0.04	5.35	0.01
<b>LW15</b>	0.04	5.56	0.01
<b>LW16</b>	0.04	5.40	0.01
<b>LW17</b>	0.04	5.59	0.01
<b>LW18</b>	0.03	5.53	0.01
<b>LW19</b>	0.04	5.77	0.01
<b>LW20</b>	0.04	5.56	0.01

### 3.2.2 Profile Evolution

For the bare and narrow vegetated dune, a laser profile was taken between  $x = 4.9 - 19.90\text{ m}$  at a cross-shore interval of  $2\text{ cm}$  in the bare zone and  $1\text{ cm}$  in the vegetation zone after each  $400 - s$  wave run because of the rapid profile changes. The scanned data in the vegetation zone had to be examined manually after automated outlier removal. The wide vegetation covering the high dune slowed down the erosion process and profile changes were small between certain wave runs. Profiles measured after runs HW4-HW6 only showed minor changes in bottom elevation. The changes were even less between HW7 and HW9. Profiles were not measured after runs 11, 12, 13, 15, 16, 18, 19, 21, 22, 24, and 25 for the HW test. As expected, the profile changed rapidly under the low and bare dune conditions. The wide vegetation for the LW test reduced the profile changes. During the LW test a laser scan was conducted after each wave run except for LW14. However, the measurements conducted after the LW1, LW15, and LW18 were unreliable in the vegetation zone and excluded from the analysis. The measured bottom elevations were averaged alongshore to obtain the beach and dune profile as a function of  $x$  and time  $t$  with  $t = 0$  at the beginning of each test.

Figures 3.7 and 3.8 show the measured profile (*elevation = 0 at SWL*) evolution in the region of noticeable profile change ( $x = 16.0 - 19.90\text{ m}$ ) in front of the vertical wall for the high and low dune test series, respectively. Each profile is identified by its run number starting from run number 0 for the initial profile. The color scale indicates the time dependent progression of the profile change from the initial (red) to the final (blue) profile measurement. The initial, intermediate and final profiles in each test are highlighted by three thick lines. Changes in the bottom elevation in the zone of  $x < 16.0\text{ m}$  were very small and are not analyzed further. Figlus et al. (2009) distinguished the profile evolution of the bare dune into three phases. During the first phase sediment eroded from the dune through scarping and slumping processes and was predominantly transported in offshore direction. The second phase encompassed the duration where wave overtopping and sediment overwash increased rapidly as a result

of the rapid dune crest lowering. During the destruction of the dune its crest was lowered to the level of the vertical wall. After the complete deconstruction a horizontal platform was all that remained from the dune. The third phase was the beach erosion in front of the vertical wall until  $SWL$  reached the vertical wall. The high dune test series in this experiment was terminated at the end of the second phase.

Figure 3.7 depicts the profile evolution of the HB (top), HN (middle), and HW (bottom) test. The profile evolutions of both the bare and narrowly vegetated high dunes were similar to the bare dune profile evolution observed by Figlus et al. (2009). The prominent rapid change in profile elevation occurred during the first run during which the rather artificial geometry of the foredune was changed and the eroded sediment was mainly transported offshore. For the HB and HN tests the wave overtopping rate  $q_o$  started to increase rapidly after 1,200 s (HB3, HN3), as discussed previously in Chapter 3.2.1. After the quick adjustment of the initial profile to the wave conditions, the profile changes slowed down. However, the dune crest was lowered continuously and the scarping and slumping processes at the dune face moved the dune crest further onshore. Backdune erosion increased due to the increase of wave overtopping. The final dune profile was a horizontal platform in front of the vertical wall at the level of the wall's crest. For the wide vegetation, however, the erosion process was slowed down noticeably. Due to the protection of the foredune against direct wave attack and scarping by the wide vegetation, overtopping did not occur until after run  $HW20$  (8,000 s) and remained small until the end of the test. The HW test was terminated when the profile differences in alongshore direction were not negligible.

Scarping was not observed during the low dune test series in Figure 3.8. It took only 1,200 s to erode the low bare dune profile to the level of the vertical wall's crest. The process was slower for the widely vegetated dune exposed to 20 wave runs. The wide vegetation covered the backdune and foredune landward of  $SWL$ . With the progression of the foredune erosion, the still water shoreline moved landward and the vegetation zone became more exposed to broken waves in the inner surf zone. At

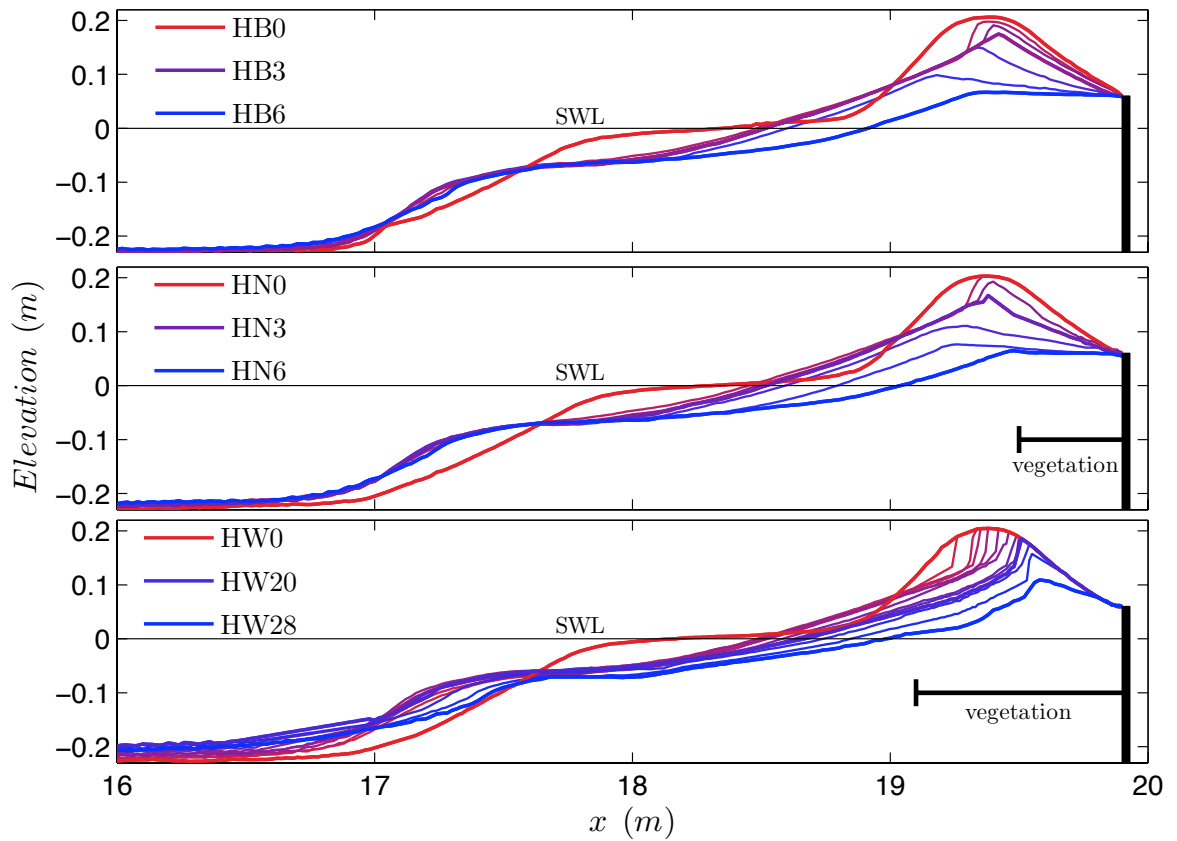


**Figure 3.7:** Dune profile evolution for HB (top), HN (middle), and HW (bottom) tests. The color scale from red (initial profile) to blue (final profile) indicates the measured profile number (HB, HN: 1 – 6; HW: 1 – 28) and the corresponding time level (HB, HN: 0 – 2, 400 s; HW: 0 – 11, 200 s).

the seaward edge, a small hump was formed in front of the seaward first row of the vegetation. Towards the end of the LW test, the tip of the vertical wall was exposed to direct wave action. The sand reinforcement effect by the buried parts (idealized roots) of the dowels appeared to be negligible for the LW test with no scarping.

Figure 3.9 shows the slumping and scarping processes during the high dune test series. Two photos (left and middle) were taken during the HW test. The third (right) photo depicts the hump formed in front of the dowels for the LW test with no scarping.

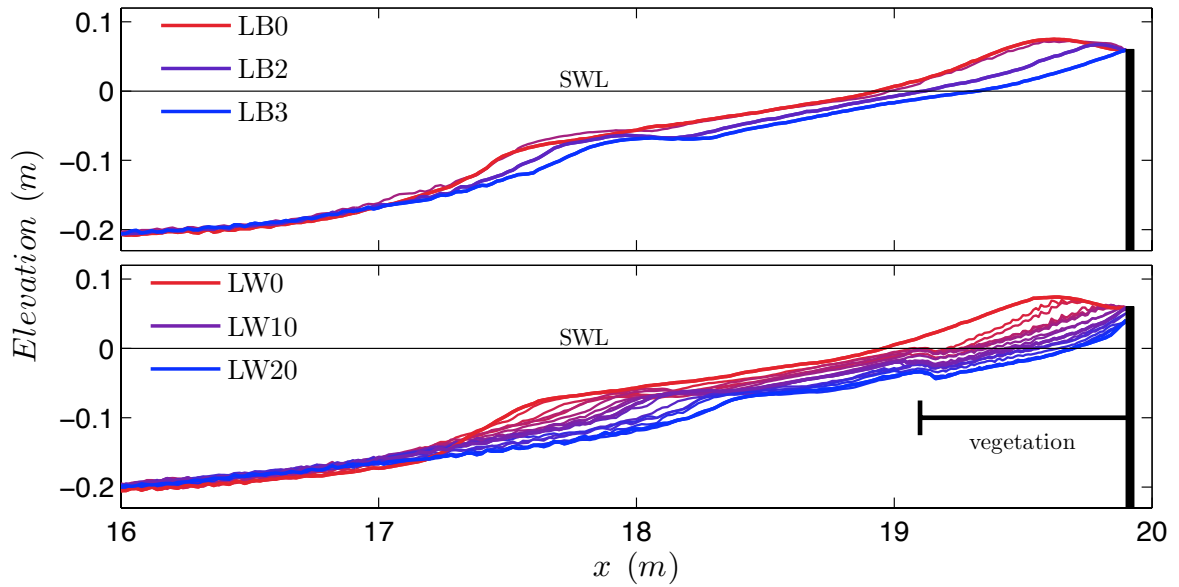


**Figure 3.8:** Dune profile evolution for LB (top), and LW (bottom) tests. The color scale from red (initial profile) to blue (final profile) indicates the measured profile number (LB: 1 – 3; LW: 1 – 20) and the corresponding time level (LB: 0 – 1, 200 s; LW: 0 – 8, 000 s).



**Figure 3.9:** Photos taken during the HW (left and middle) and LW (right) tests illustrating scarping and slumping processes for the high dune test series and the hump formed during the low dune test with the wide vegetation.

### 3.2.3 Erosion and Deposition

The sediment budget is examined for the dune and berm zone between  $x = 16.0 - 19.9 \text{ m}$ . Volumetric changes are obtained by integrating the difference between two profiles measured at different time levels over the analyzed zone. Cumulative volume changes of the profile measured at time  $t$  are computed with respect to the initial bottom profile at  $t = 0$  for each test. All values are expressed per unit width. A more detailed description of this method is given by Figlus et al. (2009). The eroded volume is subsequently compared to the overwash sand volume. The eroded and deposited volumes are chosen to be positive and negative, respectively.

Table 3.27 to 3.31 list the cumulative profile sand volume changes ( $\text{cm}^2$ ) for all five tests, respectively. Besides the values describing the cumulative eroded volume  $V_e$  and the deposited volume  $V_d$ , the total volume change  $V_c = (V_e + V_d)$  is also tabulated. All values include a void portion associated with the porosity  $n_p = 0.4$  of the sediment used in this experiment.  $V_e$  and  $V_d$  are the eroded and deposited areas relative to the initial profile in Figures 3.7 and 3.8.

The cumulative eroded volume after HB6 is  $1441 \text{ cm}^2$ . The narrow vegetation did not slow dune erosion and the eroded volume for HN6 is  $1534 \text{ cm}^2$ . Even though 28 wave bursts were generated for the HW test, the value for  $V_e$  of  $1468 \text{ cm}^2$  is similar to those for the HB and HN tests. For the low dune test series the LW test was continued for 20 runs but only 3 wave runs were generated for the LB test whose cumulative volume changes in Table 3.30 are smaller. Sediment was transported out of the system at the landward boundary due to wave overwash. That caused a decrease of sand volume contained in the zone of  $x = 16.0 - 19.9 \text{ m}$  and  $V_c$  is always positive (net erosion) toward the end of each test after the initial dune profile adjustment in the berm and dune zone.

**Table 3.27:** Cumulative values of the eroded ( $V_e$ ), deposited ( $V_d$ ) sand volume, and net erosion ( $V_c$ ) for the 6 runs of the HB test. Units are  $cm^2$  because all values are given per unit width ( $cm^3/cm$ ).

Run	Cumulative		
	$V_e$	$V_d$	$V_c$
HB1	435	-212	223
HB2	538	-214	324
HB3	612	-232	380
HB4	716	-261	455
HB5	1008	-208	800
HB6	1441	-172	1269

**Table 3.28:** Cumulative values of the eroded ( $V_e$ ), deposited ( $V_d$ ) sand volume, and net erosion ( $V_c$ ) for the 6 runs of the HN test. Units are  $cm^2$  because all values are given per unit width ( $cm^3/cm$ ).

Run	Cumulative		
	$V_e$	$V_d$	$V_c$
HN1	301	-476	-175
HN2	454	-426	27
HN3	580	-420	160
HN4	848	-386	463
HN5	1244	-351	893
HN6	1534	-358	1176

**Table 3.29:** Cumulative values of the eroded ( $V_e$ ), deposited ( $V_d$ ) sand volume, and net erosion ( $V_c$ ) for the 28 runs of the HW test. Units are  $cm^2$  because all values are given per unit width ( $cm^3/cm$ ).

Run	Cumulative		
	$V_e$	$V_d$	$V_c$
HW1	353	-404	-51
HW2	440	-427	12
HW3	391	-584	-193
HW4	488	-500	-12
HW7	461	-646	-185
HW10	602	-501	101
HW14	716	-569	147
HW17	734	-637	97
HW20	778	-706	73
HW23	911	-590	321
HW26	1189	-426	763
HW28	1468	-380	1089

**Table 3.30:** Cumulative values of the eroded ( $V_e$ ), deposited ( $V_d$ ) sand volume, and net erosion ( $V_c$ ) for the 3 runs of the LB test. Units are  $cm^2$  because all values are given per unit width ( $cm^3/cm$ ).

Run	Cumulative		
	$V_e$	$V_d$	$V_c$
LB1	57	-117	-60
LB2	412	-33	379
LB3	717	-39	678

**Table 3.31:** Cumulative values of the eroded ( $V_e$ ), deposited ( $V_d$ ) sand volume, and net erosion ( $V_c$ ) for the 20 runs of the LW test. Units are  $cm^2$  because all values are given per unit width ( $cm^3/cm$ ).

Run	Cumulative		
	$V_e$	$V_d$	$V_c$
LW1	NR	NR	NR
LW2	245	-86	159
LW3	407	-44	363
LW4	524	-91	433
LW5	432	-123	309
LW6	534	-149	385
LW7	629	-79	550
LW8	747	-109	639
LW9	792	-139	652
LW10	863	-132	731
LW11	923	-157	765
LW12	1110	-88	1022
LW13	1107	-141	966
LW14	NR	NR	NR
LW15	NR	NR	NR
LW16	1144	-120	1024
LW17	1312	-77	1235
LW18	NR	NR	NR
LW19	1439	-68	1371
LW20	1411	-89	1322

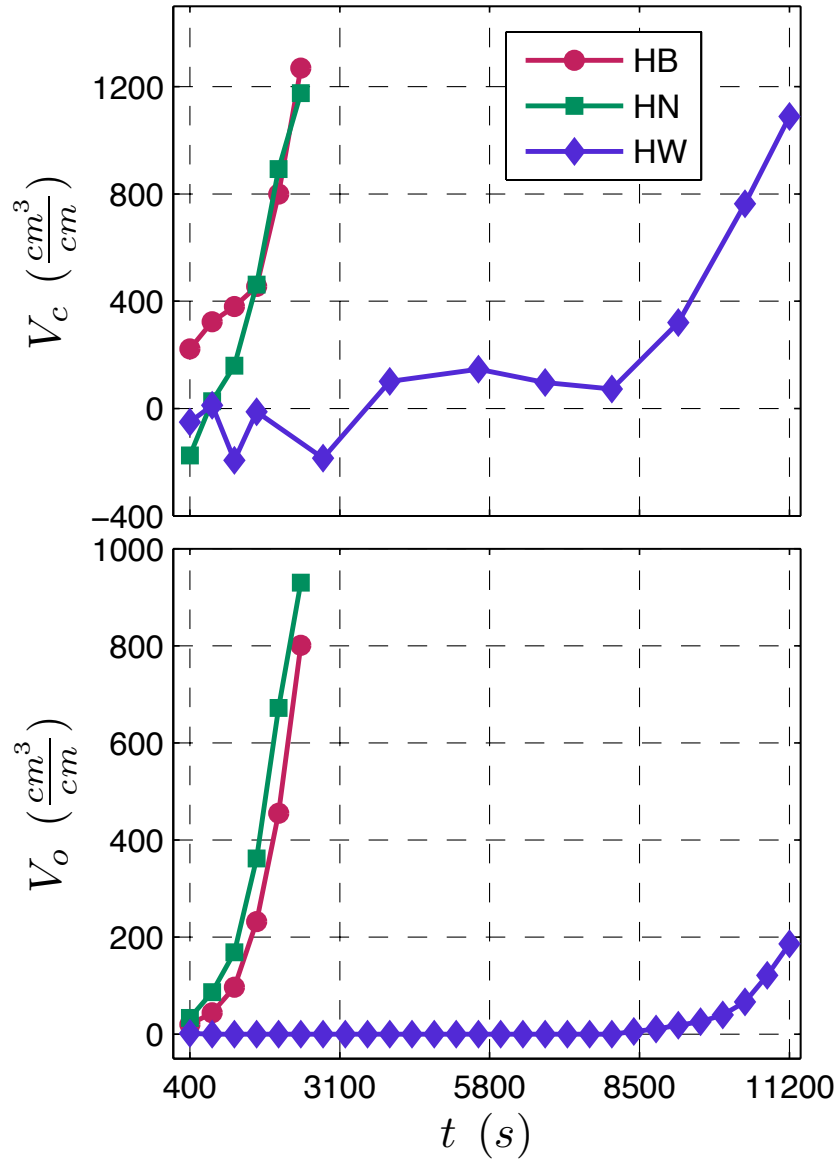
*NR implies "not reliable" data*

Table 3.32 to 3.36 list the computed cumulative volumes of overwash ( $V_o$ ), offshore loss ( $V_L$ ), and total net erosion ( $V_c$ ) and their ratios. It is noted that while the transport rates were measured for each run of the HW test, a bottom profile was not recorded for all runs in the HW test. Some profile measurements of the LW test were unreliable and excluded in this analysis. Figures 3.10 and 3.11 show the temporal variations of the cumulative volume change  $V_c$  per unit alongshore length in the top panel for the high and low dune test series, respectively. The bottom panel of both figures depicts the sand volume  $V_o$  per unit alongshore length associated with sand overwash where  $V_o$  is obtained by integrating the sand overwash rate  $q_{bs}$  from  $t = 0$  to time  $t$  at the end of each run. For the comparison of  $V_c$  and  $V_o$ , the sand porosity of 0.4 is included in  $V_o$ . The offshore loss  $V_L$  represents the sand volume that is transported offshore from the zone of  $x = 16.0 - 19.9$  m and is calculated by  $V_L(t) = V_c(t) - V_o(t)$ . Sand transported offshore is deposited in the zone of  $x = 0 - 16.0$  m. The error for the bottom elevation measurement was about 1 mm. It was not possible to measure the deposited sand volume in that region accurately. It was more accurate to estimate  $V_L$  using the values of  $V_c$  and  $V_o$  along with the conservation of sand volume in the zone of  $x = 16.0 - 19.9$  m

The values of  $V_c$  are similar at the end of all three tests of the high dune test series (Figure 3.10). In contrast to the HW (blue, diamonds) test, the HB (red, circles) and HN (green, squares) tests exhibit similar trends for  $V_c$  and  $V_o$ . Overwash did not occur for the HW test until the beginning of run HW21 and remained small until the end of the test. The total overwash volume is  $801$  cm<sup>3</sup>/cm and  $930$  cm<sup>3</sup>/cm for the HB and HN test, respectively, in comparison to  $186$  cm<sup>3</sup>/cm for the HW test. At the end of the HB, HN, and HW tests, the ratio  $V_o/V_c$  shows a value of 0.63, 0.79, and 0.17, respectively. Sand overwash over the vertical wall caused the majority of the dune erosion for the HB and HN test. The wide vegetation reduced the wave overtopping and overwash rates but increased the offshore sand loss which may be related to the increased offshore return flow resulting from the decreased wave overtopping rate. The measured undertow current at  $x = 17.1$  m was slightly larger for the HW test than for

the HB and HN tests (see Table 3.17 to 3.19). However, no measurement was made in the vegetation zone in this experiment.

Figure 3.11 shows the temporal variations of  $V_c$  and  $V_o$  for the LB and LW tests. The volume change  $V_c$  per unit alongshore length in the zone of  $x = 16.0 - 19.9 m$  increases almost linearly with time. The larger overwash rate  $q_{bs}$  leads to a higher rate of increase of  $V_c$  for the LB (red, circles) test. The cumulative overwash volume  $V_o$  attributable to  $q_{bs}$  increases with time. However, the rate of increase of  $V_o$  for the LW (blue, diamonds) test decreases with time due to the temporal decrease of  $q_{bs}$ . The observed erosion in front of the vertical wall was caused mostly by wave overtopping and overwash. At the end of the LB and LW tests, the ratio of  $V_o/V_c$  is 0.82 and 0.73, respectively. The wide vegetation reduced the wave uprush on the upward slope and wave overtopping and overwash rates. Consequently, the volumetric erosion rate was reduced in front of the vertical wall. It has to be noted that the results of the low dune test series were influenced by the vertical wall.



**Figure 3.10:** Temporal variations of cumulative sand volume change  $V_c$  (top), and overwash volume  $V_o$  (bottom) per unit width for HB, HN, and HW tests.

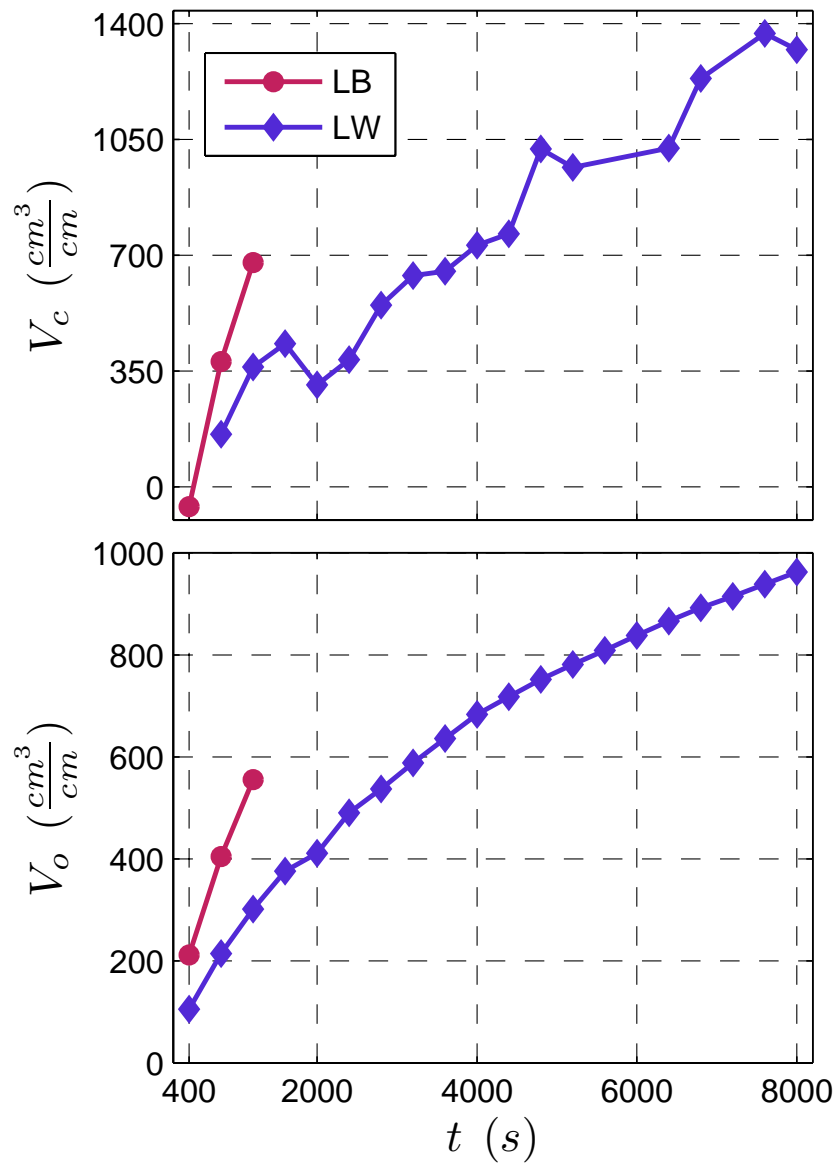


**Figure 3.11:** Temporal variations of cumulative sand volume change  $V_c$  (top), and overwash volume  $V_o$  (bottom) per unit width for LB, and LW tests.

**Table 3.32:** Measured cumulative overwash ( $V_o$ ), offshore loss ( $V_L$ ) and net erosion ( $V_c$ ) and their ratios where volumes are given per unit width ( $cm^3/cm$ ) for the 6 runs of the HB test.

Run	$V_o$	$V_L$	$V_c$	$V_L/V_c$	$V_o/V_c$
<b>HB1</b>	20	202	223	0.91	0.09
<b>HB2</b>	44	279	324	0.86	0.14
<b>HB3</b>	97	283	380	0.75	0.25
<b>HB4</b>	232	223	455	0.49	0.51
<b>HB5</b>	455	345	800	0.43	0.57
<b>HB6</b>	801	468	1269	0.37	0.63

**Table 3.33:** Measured cumulative overwash ( $V_o$ ), offshore loss ( $V_L$ ) and net erosion ( $V_c$ ) and their ratios where volumes are given per unit width ( $cm^3/cm$ ) for the 6 runs of the HN test.

Run	$V_o$	$V_L$	$V_c$	$V_L/V_c$	$V_o/V_c$
<b>HN1</b>	34	-209	-175	1.19	-0.19
<b>HN2</b>	86	-59	27	-2.19	3.19
<b>HN3</b>	169	-9	160	-0.06	1.06
<b>HN4</b>	362	101	463	0.22	0.78
<b>HN5</b>	672	221	893	0.25	0.75
<b>HN6</b>	930	246	1176	0.21	0.79

**Table 3.34:** Measured cumulative overwash ( $V_o$ ), offshore loss ( $V_L$ ) and net erosion ( $V_c$ ) and their ratios where volumes are given per unit width ( $cm^3/cm$ ) for the 28 runs of the HW test.

Run	$V_o$	$V_L$	$V_c$	$V_L/V_c$	$V_o/V_c$
HW1	2	-53	-51	1.04	-0.04
HW2	2	10	12	0.83	0.17
HW3	2	-195	-193	1.01	-0.01
HW4	2	-14	-12	1.17	-0.17
HW5	2	-	-	-	-
HW6	2	-	-	-	-
HW7	2	-187	-185	1.01	-0.01
HW8	2	-	-	-	-
HW9	2	-	-	-	-
HW10	2	99	101	0.98	0.02
HW11	2	-	-	-	-
HW12	2	-	-	-	-
HW13	2	-	-	-	-
HW14	2	145	147	0.99	0.01
HW15	2	-	-	-	-
HW16	2	-	-	-	-
HW17	2	95	97	0.98	0.02
HW18	2	-	-	-	-
HW19	2	-	-	-	-
HW20	2	71	73	0.97	0.03
HW21	6	-	-	-	-
HW22	11	-	-	-	-
HW23	18	303	321	0.94	0.06
HW24	26	-	-	-	-
HW25	40	-	-	-	-
HW26	66	97	763	0.91	0.09
HW27	121	-	-	-	-
HW28	186	903	1089	0.83	0.17

**Table 3.35:** Measured cumulative overwash ( $V_o$ ), offshore loss ( $V_L$ ) and net erosion ( $V_c$ ) and their ratios where volumes are given per unit width ( $cm^3/cm$ ) for the 3 runs of the LB test.

Run	$V_o$	$V_L$	$V_c$	$V_L/V_c$	$V_o/V_c$
<b>LB1</b>	211	-271	-60	4.54	-3.54
<b>LB2</b>	405	-26	379	-0.07	1.07
<b>LB3</b>	555	123	678	0.18	0.82

**Table 3.36:** Measured cumulative overwash ( $V_o$ ), offshore loss ( $V_L$ ) and net erosion ( $V_c$ ) and their ratios where volumes are given per unit width ( $cm^3/cm$ ) for the 20 runs of the LW test.

Run	$V_o$	$V_L$	$V_c$	$V_L/V_c$	$V_o/V_c$
<b>LW1</b>	105	NR	NR	NR	NR
<b>LW2</b>	214	-55	159	-0.34	1.34
<b>LW3</b>	302	61	363	0.17	0.83
<b>LW4</b>	376	57	433	0.13	0.87
<b>LW5</b>	411	-102	309	-0.33	1.33
<b>LW6</b>	490	-105	385	-0.27	1.27
<b>LW7</b>	537	13	550	0.02	0.98
<b>LW8</b>	588	51	639	0.08	0.92
<b>LW9</b>	636	16	652	0.02	0.98
<b>LW10</b>	683	48	731	0.06	0.94
<b>LW11</b>	718	47	765	0.06	0.94
<b>LW12</b>	752	270	1022	0.26	0.74
<b>LW13</b>	781	185	966	0.19	0.81
<b>LW14</b>	809	NR	NR	NR	NR
<b>LW15</b>	838	NR	NR	NR	NR
<b>LW16</b>	866	158	1024	0.15	0.85
<b>LW17</b>	892	343	1235	0.28	0.72
<b>LW18</b>	915	NR	NR	NR	NR
<b>LW19</b>	938	433	1371	0.32	0.68
<b>LW20</b>	963	359	1322	0.27	0.73

*NR implies "not reliable" data*



## Chapter 4

### CONCLUSIONS

Five tests were conducted to examine the effects of woody plants on dune erosion and overwash. In addition to two different dune geometries, high and low dunes, two vegetation configurations were compared with the case of no vegetation. A narrow vegetated zone covering the backdune and a wide vegetation spanning the backdune and the foredune were investigated. Vegetation was simulated by an uniform field of wooden dowels where  $2/3$  of the length of each dowel was buried into the beach sand. The same stem density was applied for all tests that included vegetation. The still water level was constant throughout the experiment at  $1.0\text{ m}$ . Hydrodynamic data for a total number of 63 of  $400 - s$  wave bursts were provided by eight capacitance wave gauges and three velocimeters. The  $3D$  bathymetry of the beach profile was recorded in high resolution by the laser line scanner system. To obtain the wave overtopping rate and sand overwash rate for each run, the water and sediment transported over the low-crested vertical wall was collected in the basin including a sediment trap.

One bare and two vegetation configurations were tested for the high dune geometry to examine the vegetation effects on erosion and scarping process occurring on the foredune as well as wave overtopping and overwash on the backdune. The wave overtopping rate and sand overwash rate were not reduced by the narrow vegetation which affected the dune evolution negligibly. However, the wide vegetation covering the backdune and foredune reduced foredune scarping, prevented wave overtopping initially, and reduced the overtopping and overwash rates after the initiation of wave overtopping. Due to the reduction of overtopping and overwash, sediment eroded from the dune was transported mostly offshore on the basis of the sediment volume change in the dune zone. Since the high dune test series showed that the narrow vegetation

did not enhance the dune resilience against destruction by wave-induced overwash, the low dune was tested under bare and wide vegetation conditions only. These two tests examined the vegetation effects in the absence of foredune scarping. The dune erosion was reduced by the wide vegetation because the vegetation retarded wave uprush on the upward slope in the swash and inner surf zones and reduced the wave overtopping and overwash rates. However, observations during the high and low test series indicated that the vegetation might have increased the sand mobilization in the vegetation zone.

The results of this investigation may be useful in designing a vegetation zone to reduce dune overwash. However, it has to be noted that this study was limited to the specific diameter, height, spacing, alignment, and burial depth of rigid wooden dowels. Additional experiments are necessary to test different configurations. Furthermore, a large-scale experiment is also required to quantify scale effects in the present small-scale experiment. Wooden dowels may not represent roots, trunks, branches, and leaves adequately. Additionally, woody plants could be destroyed by the wave force or uprooted due to erosion in the field. These factors were not considered in this experiment. Furthermore, it has to be noted that the results of the low dune test series were influenced by the vertical wall. Additional tests are required for low dunes without scarping in the absence of the vertical wall. Nevertheless, the present experimental results will be useful for the initial development of a numerical model for vegetated dune overwash.

## REFERENCES

- Acuity (2003). *AccuRange 1000 laser distance sensor user's manual*. Schmitt Measurement System, Inc.
- Algera, A. (2006). *Run-up reduction through vetiver grass*. Final Report, Master Thesis, Delft University of Technology, Delft.
- Asano, T. (2008). *Evaluation of tsunami attenuation performance of coastal forests based on tree morphology*. Proc. 31st Coastal Engineering Conf., World Scientific, Singapore, 1446-1457.
- Asano, T., Deguchi, H., and Kobayashi, N. (1992). *Interaction between water waves and vegetation*. Proc. 23rd Coastal Engineering Conf., ASCE, Reston, Va., 2710-2723.
- Augustin, L.N., Irish, J.L., and Lynett, P. (2009). *Laboratory and numerical studies of wave damping by emergent and near-emergent wetland vegetation*. Coastal Eng., 56, 332-340.
- Bender, C.J., Atkinson, J., Cialone, M.A., Grzegorzewski, A., and Smith, J.M. (2008). *Numerical simulation of the effects of Louisiana coastal marshes on nearshore waves*. Proc. 31st Coastal Engineering Conf., World Scientific, Singapore, 1012-1023.
- Buck, M., Kobayashi, N., Payo, A, and Johnson, B.D. (2007). *Berm and Dune Erosion during a Storm*. Research Report CACR-07-03, University of Delaware Center for Applied Coastal Research, Newark, Del.
- Crowell, M., Coulton, K., Johnson, C., Westscott, J., Bellomo, D., Edelman, C., and Hirsch, E. (2010). *An estimate of the U.S. population living in 100-year coastal flood hazard areas*. J. Coastal Res., 26(2), 201-211.
- Dean, R.G. and Bender, C.J. (2006). *Static wave setup with emphasis on damping effects by vegetation and bottom friction*. Coastal Eng., 53, 149-156.

- Dalrymple, R.A., Kirby, J.T., and Hwang, P.A. (1984). *Wave diffraction due to areas of energy dissipation*. J. Waterway, Port, Coastal, Ocean Eng., 110(1), 67-79.
- Donnelly, C., Kraus, N., and Larson, M. (2006). *State of knowledge on measurement and modeling of coastal overwash*. J. Coastal Res., 22(4), 965-991.
- Figlus, J., Kobayashi N., Gralher, C., and Iranzo V.(2009). *Experimental and Numerical Study on the Transition from Minor to Major Overwash of Dunes*. Research Report CACR-09-04, University of Delaware Center for Applied Coastal Research, Newark, Del.
- Gutierrez, B.T., Williams, S.J., and Thieler, E.R. (2007). *Potential for shoreline changes due to sea-level rise along the U.S. Mid-Atlantic Region*. Open-File Report 2007-1278, U.S. Geological Survey, <http://pubs.usgs.gov/of/2007/1278>.
- Hayashi, K., Hashimoto, K., Yagisawa, K., and Kobayashi, N. (2010). *Beach morphologies at Notsukezaki sand spit, Japan*. Proc. 32nd Coastal Engineering Conf., Sediments 48, 1-12.
- Judge, E.K, Overton, M.F., and Fisher, J.S. (2003). *Vulnerability indicators of coastal dunes*. J. Waterway, Port, Coastal, Ocean Eng., 129(6), 270-278.
- Kobayashi, N., Raichle, A., and Ansano, T. (1993). *Wave attenuation by vegetation*. J. Waterway, Port, Coastal, Ocean Eng., 119(1), 30-48.
- Leatherman, S.P. (1981). *Overwash Processes*. Benchmark Papers in Geology, Hutchinson Ross Company, USA.
- Løvås, S.M., and Tørum, A. (2001). *Effect of the kelp *Laminaria hyperborean* upon sand dune erosion and water particle velocities*. J. Waterway, Port, Coastal, Ocean Eng., 119(1), 30-48.
- Méndez, F., Losada, I.J., and Losada, M.A. (1999). *Hydrodynamics induced by wind waves in a vegetation field*. J. Geophys. Res., 104(C8), 18,383-18,396.
- Resio, D.T., and Westerwick, J.J. (2008) *Modeling the physics of storm surges*. Physics Today, 61(9), 33-38.
- Rosati, J.D., and Stone, G.W. (2009) *Geomorphologic evolution of barrier islands along the northern U.S. Gulf of Mexico and implications for engineering design in barrier restoration*. J. Coastal Res., 25(1), 8-22.

Rusello, P.J. (2009). *A Practical Primer for Pulse Coherent Instruments*. Technical Note, Nortek, USA.

Wang, P., Kirby, J.H., Haber, J.D., Horwitz, M.H., Knorr, P.O., and Krock, J.R. (2006). *Morphological and sedimentological impacts of Hurricanes Ivan and immediate poststorm beach recovery along the northwestern Florida barrier-island coasts*. *J. Coastal Res.*, 22(6), 1382-1402.

**Internet sources:**

Nortek AS (2009). *Product Information*. Available from: <http://www.nortek-as.com/> (Accessed November 2009).

United Nations Atlas of the Oceans (2012). *Human Settlements on the Coast*. Available from: <http://www.oceansatlas.org/id/1877> (Accessed May 2012).



**Appendix**  
**TABULATED DATA**

**Table A.1:** Spectrum and time series parameters for total waves at WG1 ( $x = 0\text{ m}$ ) for the 6 runs of the HB test.

<b>Run</b>	<b><math>H_{mo}</math> (cm)</b>	<b><math>H_{rms}</math> (cm)</b>	<b><math>H_s</math> (cm)</b>	<b><math>T_p</math> (s)</b>	<b><math>T_s</math> (s)</b>
<b>HB1</b>	18.29	12.93	17.80	2.39	2.29
<b>HB2</b>	18.79	13.29	18.63	2.70	2.30
<b>HB3</b>	18.66	13.19	18.46	2.70	2.31
<b>HB4</b>	18.64	13.18	18.33	2.70	2.29
<b>HB5</b>	18.65	13.19	18.45	2.70	2.32
<b>HB6</b>	18.41	13.02	18.20	2.57	2.30
Average	18.57	13.13	18.31	2.62	2.30

**Table A.2:** Spectrum and time series parameters for total waves at WG1 ( $x = 0\text{ m}$ ) for the 6 runs of the HN test.

<b>Run</b>	<b><math>H_{mo}</math> (cm)</b>	<b><math>H_{rms}</math> (cm)</b>	<b><math>H_s</math> (cm)</b>	<b><math>T_p</math> (s)</b>	<b><math>T_s</math> (s)</b>
<b>HN1</b>	18.38	13.00	17.73	2.39	2.28
<b>HN2</b>	18.70	13.22	18.50	2.57	2.31
<b>HN3</b>	18.52	13.10	18.16	2.64	2.29
<b>HN4</b>	18.98	13.42	17.92	2.57	2.26
<b>HN5</b>	18.89	13.36	18.63	2.57	2.33
<b>HN6</b>	18.31	12.95	18.17	2.57	2.31
Average	18.63	13.17	18.19	2.55	2.30

**Table A.3:** Spectrum and time series parameters for total waves at WG1 ( $x = 0$  m) for the 28 runs of the HW test.

Run	$H_{mo}$ (cm)	$H_{rms}$ (cm)	$H_s$ (cm)	$T_p$ (s)	$T_s$ (s)
HW1	18.16	12.84	17.81	2.57	2.28
HW2	18.30	12.94	17.83	2.57	2.30
HW3	18.61	13.16	18.29	2.57	2.31
HW4	18.44	13.04	18.28	2.57	2.33
HW5	18.51	13.09	18.24	2.57	2.29
HW6	18.43	13.03	18.02	2.57	2.30
HW7	18.51	13.09	18.22	2.57	2.31
HW8	18.57	13.13	18.37	2.57	2.32
HW9	18.63	13.17	18.20	2.57	2.27
HW10	18.63	13.17	18.46	2.57	2.32
HW11	18.77	13.28	18.35	2.57	2.29
HW12	18.84	13.32	18.75	2.57	2.31
HW13	18.90	13.36	18.73	2.57	2.32
HW14	18.94	13.39	18.79	2.57	2.31
HW15	18.45	13.03	18.18	2.57	2.32
HW16	18.61	13.16	18.40	2.57	2.31
HW17	18.60	13.15	18.28	2.57	2.31
HW18	18.30	12.94	18.14	2.57	2.31
HW19	18.45	13.05	18.23	2.57	2.33
HW20	18.50	13.08	18.19	2.57	2.30
HW21	18.39	13.01	18.12	2.57	2.32
HW22	18.47	13.06	18.19	2.57	2.33
HW23	18.42	13.03	18.20	2.57	2.31
HW24	18.00	12.73	17.68	2.57	2.35
HW25	18.13	12.82	17.92	2.57	2.33
HW26	18.31	12.95	18.02	2.57	2.33
HW27	18.14	12.83	17.74	2.57	2.32
HW28	18.10	12.80	17.86	2.57	2.34
Average	18.57	13.06	18.20	2.57	2.31

**Table A.4:** Spectrum and time series parameters for total waves at WG1 ( $x = 0\text{ m}$ ) for the 3 runs of the LB test.

Run	$H_{mo}$ (cm)	$H_{rms}$ (cm)	$H_s$ (cm)	$T_p$ (s)	$T_s$ (s)
<b>LB1</b>	17.91	12.66	16.87	2.57	2.27
<b>LB2</b>	17.65	12.48	17.31	2.57	2.32
<b>LB3</b>	18.10	12.80	17.62	2.57	2.31
Average	17.89	12.65	17.26	2.57	2.30

**Table A.5:** Spectrum and time series parameters for total waves at WG1 ( $x = 0\text{ m}$ ) for the 20 runs of the LW test.

Run	$H_{mo}$ (cm)	$H_{rms}$ (cm)	$H_s$ (cm)	$T_p$ (s)	$T_s$ (s)
<b>LW1</b>	17.93	12.68	17.57	2.57	2.31
<b>LW2</b>	19.95	14.11	19.79	2.57	2.27
<b>LW3</b>	19.91	14.08	19.54	2.57	2.31
<b>LW4</b>	18.33	12.96	17.85	2.57	2.30
<b>LW5</b>	17.95	12.69	17.73	2.57	2.28
<b>LW6</b>	18.28	12.93	17.84	2.57	2.28
<b>LW7</b>	18.22	12.89	17.90	2.57	2.31
<b>LW8</b>	18.22	12.89	17.90	2.57	2.31
<b>LW9</b>	18.60	13.15	18.29	2.57	2.30
<b>LW10</b>	18.63	13.17	18.33	2.57	2.31
<b>LW11</b>	18.92	13.38	18.94	2.57	2.33
<b>LW12</b>	18.56	13.12	18.28	2.57	2.32
<b>LW13</b>	17.56	12.42	17.36	2.57	2.31
<b>LW14</b>	18.72	13.24	18.50	2.57	2.31
<b>LW15</b>	18.51	13.09	18.30	2.57	2.31
<b>LW16</b>	18.39	13.01	18.20	2.57	2.32
<b>LW17</b>	18.45	13.05	18.28	2.57	2.31
<b>LW18</b>	18.52	13.09	18.35	2.57	2.34
<b>LW19</b>	18.69	13.21	18.64	2.57	2.33
<b>LW20</b>	18.73	13.25	18.59	2.57	2.32
Average	18.55	13.12	18.31	2.57	2.31

**Table A.6:** Mean cross-shore  $\bar{u}$ , and alongshore  $\bar{v}$  velocity and their standard deviations of the 2D ADV co-located with WG5 at  $x = 12.90$  m for the HB test.

Run	$\bar{u}$ (cm/s)	$\sigma_u$ (cm/s)	$\bar{v}$ (cm/s)	$\sigma_v$ (cm/s)
<b>HB1</b>	-4.92	17.61	-0.25	2.92
<b>HB2</b>	-5.49	17.64	-0.91	2.78
<b>HB3</b>	-5.72	17.40	-0.34	2.90
<b>HB4</b>	-5.31	17.45	-0.57	2.73
<b>HB5</b>	-4.66	17.38	-0.41	2.96
<b>HB6</b>	-3.73	16.81	-0.87	3.00

**Table A.7:** Mean cross-shore  $\bar{u}$ , and alongshore  $\bar{v}$  velocity and their standard deviations of the 2D ADV co-located with WG5 at  $x = 12.90$  m for the HN test.

Run	$\bar{u}$ (cm/s)	$\sigma_u$ (cm/s)	$\bar{v}$ (cm/s)	$\sigma_v$ (cm/s)
<b>HN1</b>	-4.80	18.58	-0.99	3.20
<b>HN2</b>	-6.60	18.27	-0.32	3.16
<b>HN3</b>	-5.28	18.36	-0.49	3.30
<b>HN4</b>	-5.91	18.26	-0.98	3.26
<b>HN5</b>	-4.92	18.00	-1.19	3.19
<b>HN6</b>	-3.91	17.65	-0.41	3.63

**Table A.8:** Mean cross-shore  $\bar{u}$ , and alongshore  $\bar{v}$  velocity and their standard deviations of the 2D ADV co-located with WG5 at  $x = 12.90$  m for the HW test.

Run	$\bar{u}$ (cm/s)	$\sigma_u$ (cm/s)	$\bar{v}$ (cm/s)	$\sigma_v$ (cm/s)
HW1	-4.71	18.11	-0.10	3.45
HW2	-5.10	18.24	-0.48	3.58
HW3	-5.46	18.29	-0.33	2.99
HW4	-4.79	17.98	-1.19	2.91
HW5	-5.17	18.01	0.08	3.28
HW6	-5.37	17.94	-0.33	3.26
HW7	NR	NR	NR	NR
HW8	-4.98	17.79	-0.87	3.10
HW9	-5.24	17.69	-0.31	2.93
HW10	-5.14	17.81	-0.59	2.99
HW11	-5.69	17.11	0.74	3.12
HW12	-5.20	17.59	-0.62	2.87
HW13	-6.00	17.53	-0.07	3.15
HW14	-5.68	17.32	-0.60	3.03
HW15	-4.68	17.43	-0.06	3.38
HW16	-5.84	17.63	-0.36	3.04
HW17	-5.36	17.32	-0.24	3.00
HW18	-4.85	17.09	-0.32	2.94
HW19	-5.87	16.84	-0.50	3.23
HW20	-5.12	17.00	-0.20	3.20
HW21	-4.72	16.80	-0.07	2.89
HW22	-5.08	17.00	-0.63	3.08
HW23	-5.75	17.10	-0.72	2.99
HW24	-5.28	17.17	-0.06	2.96
HW25	-5.00	16.83	-0.52	3.12
HW26	-6.26	17.00	0.00	3.03
HW27	-4.24	17.01	0.01	3.10
HW28	-4.84	16.98	-0.23	3.06

*NR implies "not reliable" data*

**Table A.9:** Mean cross-shore  $\bar{u}$ , and alongshore  $\bar{v}$  velocity and their standard deviations of the 2D ADV co-located with WG5 at  $x = 12.90$  m for the LB test.

Run	$\bar{u}$ (cm/s)	$\sigma_u$ (cm/s)	$\bar{v}$ (cm/s)	$\sigma_v$ (cm/s)
<b>LB1</b>	-4.31	16.68	-0.28	3.15
<b>LB2</b>	-4.48	16.83	-0.31	2.86
<b>LB3</b>	-5.21	16.62	-0.63	2.83

**Table A.10:** Mean cross-shore  $\bar{u}$ , and alongshore  $\bar{v}$  velocity and their standard deviations of the 2D ADV co-located with WG5 at  $x = 12.90$  m for the LW test.

Run	$\bar{u}$ (cm/s)	$\sigma_u$ (cm/s)	$\bar{v}$ (cm/s)	$\sigma_v$ (cm/s)
<b>LW1</b>	-5.42	17.04	0.13	2.91
<b>LW2</b>	-5.76	17.30	-0.43	2.90
<b>LW3</b>	-5.22	17.10	-0.60	3.11
<b>LW4</b>	-5.15	16.99	-0.19	2.84
<b>LW5</b>	-5.18	17.08	-0.28	3.10
<b>LW6</b>	-6.42	17.26	-0.03	3.04
<b>LW7</b>	-5.97	16.74	-0.28	2.82
<b>LW8</b>	-4.28	15.83	-0.20	3.04
<b>LW9</b>	-4.90	17.06	-0.43	3.18
<b>LW10</b>	-4.69	17.02	0.21	3.15
<b>LW11</b>	-6.17	16.88	0.20	2.97
<b>LW12</b>	-4.43	15.88	-0.29	2.69
<b>LW13</b>	-5.13	16.69	-0.29	2.74
<b>LW14</b>	-6.12	17.05	-0.35	2.76
<b>LW15</b>	-5.95	17.06	-0.04	3.03
<b>LW16</b>	-5.49	17.32	-0.03	2.94
<b>LW17</b>	-4.73	17.01	-0.50	3.05
<b>LW18</b>	-4.80	16.88	-0.85	2.92
<b>LW19</b>	-5.84	17.15	0.02	2.70
<b>LW20</b>	-5.98	17.09	-0.56	2.96

**Table A.11:** Mean cross-shore  $\bar{u}$ , alongshore  $\bar{v}$ , and vertical  $\bar{w}$  velocity and their standard deviations of the blue Vectrino co-located with WG6 at  $x = 15.52 m$  for the HB test.

Run	$\bar{u}$ (cm/s)	$\sigma_u$ (cm/s)	$\bar{v}$ (cm/s)	$\sigma_v$ (cm/s)	$\bar{w}$ (cm/s)	$\sigma_w$ (cm/s)
HB1	-3.35	16.68	0.53	4.40	-0.52	4.83
HB2	-2.92	17.29	0.07	3.28	-1.03	4.99
HB3	-3.73	17.27	0.09	2.70	-0.73	3.59
HB4	-3.74	17.07	0.60	3.34	-0.92	4.18
HB5	-2.84	16.84	0.36	2.74	-1.08	4.20
HB6	-3.07	16.89	-0.02	2.32	-0.64	4.34

**Table A.12:** Mean cross-shore  $\bar{u}$ , alongshore  $\bar{v}$ , and vertical  $\bar{w}$  velocity and their standard deviations of the blue Vectrino co-located with WG6 at  $x = 15.52 m$  for the HN test.

Run	$\bar{u}$ (cm/s)	$\sigma_u$ (cm/s)	$\bar{v}$ (cm/s)	$\sigma_v$ (cm/s)	$\bar{w}$ (cm/s)	$\sigma_w$ (cm/s)
HN1	-4.73	17.97	0.70	2.64	-0.77	3.79
HN2	-4.39	18.17	0.33	3.31	-0.64	3.65
HN3	-4.40	18.42	-0.11	2.51	-0.83	4.51
HN4	-4.87	18.31	-0.56	2.97	-1.16	4.47
HN5	-3.85	18.10	0.03	2.57	-1.21	4.28
HN6	-3.73	17.78	-0.56	2.98	-0.17	4.41

**Table A.13:** Mean cross-shore  $\bar{u}$ , alongshore  $\bar{v}$ , and vertical  $\bar{w}$  velocity and their standard deviations of the blue Vectrino co-located with WG6 at  $x = 15.52\text{ m}$  for the HW Test.

Run	$\bar{u}$ (cm/s)	$\sigma_u$ (cm/s)	$\bar{v}$ (cm/s)	$\sigma_v$ (cm/s)	$\bar{w}$ (cm/s)	$\sigma_w$ (cm/s)
HW1	NR	NR	NR	NR	NR	NR
HW2	-4.19	18.03	0.34	2.70	-1.07	4.19
HW3	NR	NR	NR	NR	NR	NR
HW4	-4.10	18.53	-0.29	2.42	-0.98	4.08
HW5	-4.22	18.43	-0.11	2.28	-1.06	4.00
HW6	-3.69	18.24	0.13	2.63	-1.17	4.60
HW7	NR	NR	NR	NR	NR	NR
HW8	-4.09	18.16	0.33	2.69	-1.21	4.44
HW9	-3.76	18.04	-0.17	2.63	-1.09	5.00
HW10	-3.93	18.05	0.14	2.29	-1.10	4.33
HW11	NR	NR	NR	NR	NR	NR
HW12	-3.49	17.92	0.08	2.41	-1.26	4.48
HW13	-4.16	17.78	-0.11	2.37	-1.38	4.28
HW14	-4.30	17.67	-0.29	2.33	-1.18	4.06
HW15	-4.22	17.74	0.54	3.06	-1.31	4.48
HW16	-3.74	17.77	0.52	3.07	-1.34	4.43
HW17	-4.03	17.58	0.44	3.08	-1.23	4.43
HW18	-4.03	17.65	0.09	2.41	-1.27	4.27
HW19	-3.94	17.79	-0.01	2.42	-1.02	4.09
HW20	-4.11	17.88	-0.29	2.30	-0.99	4.04
HW21	-3.84	17.80	0.52	3.02	-1.19	4.21
HW22	-4.01	17.72	0.65	2.99	-1.32	4.22
HW23	-4.08	17.56	-0.01	2.73	-1.13	3.91
HW24	-3.56	17.39	0.34	2.48	-1.22	4.93
HW25	-4.35	17.51	-0.15	2.40	-1.15	4.65
HW26	-3.94	17.26	-0.36	2.39	-1.31	4.59
HW27	-4.38	17.36	-0.12	2.34	-1.30	4.32
HW28	-3.84	17.01	0.29	3.07	-1.19	4.50

*NR implies "not reliable" data*

**Table A.14:** Mean cross-shore  $\bar{u}$ , alongshore  $\bar{v}$ , and vertical  $\bar{w}$  velocity and their standard deviations of the blue Vectrino co-located with WG6 at  $x = 15.52 m$  for the LB test.

Run	$\bar{u}$ (cm/s)	$\sigma_u$ (cm/s)	$\bar{v}$ (cm/s)	$\sigma_v$ (cm/s)	$\bar{w}$ (cm/s)	$\sigma_w$ (cm/s)
<b>LB1</b>	-3.96	16.89	0.15	2.64	-1.27	4.34
<b>LB2</b>	-2.77	16.77	0.12	2.55	-1.29	4.69
<b>LB3</b>	NR	NR	NR	NR	NR	NR

*NR implies "not reliable" data*

**Table A.15:** Mean cross-shore  $\bar{u}$ , alongshore  $\bar{v}$ , and vertical  $\bar{w}$  velocity and their standard deviations of the blue Vectrino at co-located with WG6 at  $x = 15.52 m$  for the LW Test.

Run	$\bar{u}$ (cm/s)	$\sigma_u$ (cm/s)	$\bar{v}$ (cm/s)	$\sigma_v$ (cm/s)	$\bar{w}$ (cm/s)	$\sigma_w$ (cm/s)
LW1	-3.91	17.15	0.30	3.20	-0.97	4.27
LW2	-3.27	17.14	-0.28	2.52	-1.05	4.77
LW3	-4.20	16.81	-0.08	2.37	-1.18	4.72
LW4	NR	NR	NR	NR	NR	NR
LW5	-3.60	16.95	-0.19	2.29	-1.00	4.50
LW6	-3.65	16.69	-0.29	2.69	-1.11	5.10
LW7	-3.35	17.06	-0.66	2.58	-0.90	4.40
LW8	-3.39	16.98	-0.07	2.37	-1.08	4.75
LW9	-2.64	16.86	0.32	3.10	-0.97	4.75
LW10	-4.08	16.71	-0.18	2.33	-1.29	4.33
LW11	-3.56	16.83	0.15	2.63	-1.45	4.34
LW12	-3.70	17.15	0.09	2.69	-0.86	4.47
LW13	-3.94	17.19	-0.09	2.18	-1.41	4.63
LW14	NR	NR	NR	NR	NR	NR
LW15	-3.05	17.17	-0.25	2.84	-1.18	4.89
LW16	-2.91	17.21	-0.48	2.65	-0.91	4.38
LW17	-3.92	17.20	-0.10	2.67	-0.95	4.55
LW18	NR	NR	NR	NR	NR	NR
LW19	-3.52	17.00	-0.24	2.84	-0.92	4.34
LW20	-3.36	17.20	-0.28	2.44	-1.12	4.54

*NR implies "not reliable" data*

**Table A.16:** Mean cross-shore  $\bar{u}$ , alongshore  $\bar{v}$ , and vertical  $\bar{w}$  velocity and their standard deviations of the red Vectrino co-located with WG7 at  $x = 17.07$  m for the HB test.

Run	$\bar{u}$ (cm/s)	$\sigma_u$ (cm/s)	$\bar{v}$ (cm/s)	$\sigma_v$ (cm/s)	$\bar{w}$ (cm/s)	$\sigma_w$ (cm/s)
HB1	-3.64	19.20	0.08	3.30	-0.84	5.76
HB2	-3.86	19.69	-0.35	3.12	-1.63	6.00
HB3	-4.76	19.78	-0.48	3.53	-1.83	5.99
HB4	-3.97	20.60	-0.24	3.41	-1.77	6.47
HB5	-4.84	20.97	-0.82	3.31	-1.79	6.09
HB6	-3.42	20.39	-0.32	2.89	-1.50	5.73

**Table A.17:** Mean cross-shore  $\bar{u}$ , alongshore  $\bar{v}$ , and vertical  $\bar{w}$  velocity and their standard deviations of the red Vectrino co-located with WG7 at  $x = 17.07$  m for the HN test.

Run	$\bar{u}$ (cm/s)	$\sigma_u$ (cm/s)	$\bar{v}$ (cm/s)	$\sigma_v$ (cm/s)	$\bar{w}$ (cm/s)	$\sigma_w$ (cm/s)
HN1	-4.50	19.91	-0.62	4.26	-1.65	6.30
HN2	-5.63	20.88	-0.19	4.19	-2.71	6.48
HN3	-4.89	21.34	-0.23	3.91	-2.39	7.05
HN4	-4.60	20.53	-0.19	3.59	-2.37	6.46
HN5	-3.99	20.31	-1.08	3.68	-1.76	5.98
HN6	-3.47	19.13	-0.58	2.91	-1.23	5.13

**Table A.18:** Mean cross-shore  $\bar{u}$ , alongshore  $\bar{v}$ , and vertical  $\bar{w}$  velocity and their standard deviations of the red Vectrino co-located with WG7 at  $x = 17.07\text{ m}$  for the HW test.

Run	$\bar{u}$ (cm/s)	$\sigma_u$ (cm/s)	$\bar{v}$ (cm/s)	$\sigma_v$ (cm/s)	$\bar{w}$ (cm/s)	$\sigma_w$ (cm/s)
HW1	-4.32	19.36	0.06	3.81	-0.91	5.06
HW2	-5.67	21.67	0.37	3.69	-2.44	6.66
HW3	-5.60	22.76	-0.77	3.77	-2.57	7.38
HW4	-5.81	21.35	0.19	3.89	-2.74	8.76
HW5	-5.41	23.56	-0.01	4.04	-2.25	7.72
HW6	-5.75	23.78	-0.53	3.94	-2.36	8.06
HW7	NR	NR	NR	NR	NR	NR
HW8	-5.80	23.40	0.26	4.08	-2.35	7.25
HW9	-5.22	23.09	-0.32	3.95	-2.18	6.98
HW10	-5.98	23.83	-0.41	4.00	-2.14	7.08
HW11	-6.13	23.52	0.04	4.16	-2.63	6.70
HW12	-5.22	23.54	NR	NR	NR	NR
HW13	-5.04	22.38	-0.09	4.39	-2.29	6.47
HW14	-4.99	22.09	-0.33	3.93	-2.45	6.59
HW15	-5.30	22.13	0.62	3.87	-2.46	6.08
HW16	-5.41	21.44	-0.07	3.91	-2.20	5.92
HW17	-5.75	21.51	-0.48	4.00	-2.09	5.86
HW18	-4.67	21.57	-0.23	3.73	-1.90	6.07
HW19	-4.83	21.32	0.09	3.72	-1.86	5.73
HW20	NR	NR	NR	NR	NR	NR
HW21	-4.71	21.27	-0.47	3.47	-1.45	5.20
HW22	-4.41	21.34	-0.43	3.31	-1.51	5.22
HW23	-4.90	21.37	0.12	3.42	-1.61	5.30
HW24	-4.47	21.13	-1.14	3.64	-1.26	4.89
HW25	-4.36	21.14	-0.03	3.53	-1.36	5.00
HW26	NR	NR	NR	NR	NR	NR
HW27	-4.50	21.10	-0.21	3.14	-1.36	5.35
HW28	-4.44	20.60	-0.47	3.40	-1.44	5.14

*NR implies "not reliable" data*

**Table A.19:** Mean cross-shore  $\bar{u}$ , alongshore  $\bar{v}$ , and vertical  $\bar{w}$  velocity and their standard deviations of the red Vectrino co-located with WG7 at  $x = 17.07 m$  for the LB test.

Run	$\bar{u}$ (cm/s)	$\sigma_u$ (cm/s)	$\bar{v}$ (cm/s)	$\sigma_v$ (cm/s)	$\bar{w}$ (cm/s)	$\sigma_w$ (cm/s)
<b>LB1</b>	-3.99	20.23	-0.14	3.03	-0.98	4.32
<b>LB2</b>	NR	NR	NR	NR	NR	NR
<b>LB3</b>	NR	NR	NR	NR	NR	NR

*NR implies "not reliable" data*

**Table A.20:** Mean cross-shore  $\bar{u}$ , alongshore  $\bar{v}$ , and vertical  $\bar{w}$  velocity and their standard deviations of the red Vectrino co-located with WG7 at  $x = 17.07\text{ m}$  for the LW test.

Run	$\bar{u}$ (cm/s)	$\sigma_u$ (cm/s)	$\bar{v}$ (cm/s)	$\sigma_v$ (cm/s)	$\bar{w}$ (cm/s)	$\sigma_w$ (cm/s)
LW1	-5.34	19.61	0.18	2.86	-0.96	4.30
LW2	-4.47	20.07	-0.55	3.28	-1.01	4.75
LW3	-4.65	20.18	-0.34	2.61	-1.05	4.63
LW4	-4.64	20.10	-0.26	2.80	-0.98	4.48
LW5	-4.40	20.00	-1.06	3.02	-1.00	4.78
LW6	-4.70	19.96	-0.89	2.92	-1.06	4.40
LW7	-4.42	19.98	-0.56	3.09	-0.93	4.22
LW8	-4.49	20.52	-0.20	3.10	-0.95	4.18
LW9	-4.07	19.85	-0.67	3.20	-0.92	4.46
LW10	-4.35	20.07	0.31	2.80	-0.94	4.51
LW11	-3.84	19.72	-0.70	3.17	-1.16	4.59
LW12	NR	NR	NR	NR	NR	NR
LW13	-4.58	19.75	0.13	2.73	-0.90	4.22
LW14	-4.63	20.01	-0.66	2.78	-1.10	4.42
LW15	-4.22	20.03	-0.74	3.12	-0.88	4.54
LW16	-4.16	20.02	-0.48	2.93	-0.83	4.53
LW17	-4.03	19.68	-0.30	3.05	-0.83	4.38
LW18	-4.29	19.28	-0.18	2.75	-0.99	4.39
LW19	-4.49	19.20	-0.61	3.06	-0.90	4.42
LW20	-4.01	19.17	-0.87	3.08	-0.88	4.40

*NR implies "not reliable" data*